*hydrology*

MDPI

*Article*

# Estimating Reservoir Evaporation Under Mediterranean Climate Using Indirect Methods: A Case Study in Southern Portugal

**Carlos Miranda Rodrigues [1], Rita Cabral Guimarães [1,*] and Madalena Moreira [2]**

[1] MED Mediterranean Institute for Agriculture, Environment and Development & CHANGE Global Change and Sustainability Institute, Departamento de Engenharia Rural, Escola de Ciências e Tecnologia, Universidade de Évora, Polo da Mitra, Nª Srª da Tourega, 7000-083 Évora, Portugal; camr@uevora.pt

[2] MED Mediterranean Institute for Agriculture, Environment and Development & CHANGE Global Change and Sustainability Institute, Departamento de Arquitectura, Escola de Artes, Universidade Évora, Antiga Fábrica Leões, Estrada dos Leões, 7000-208 Évora, Portugal; mmvmv@uevora.pt

* Correspondence: rcg@uevora.pt

## Abstract

This study focuses on the Alentejo and Algarve regions of southern Portugal, which is characterized by a typical Mediteranean climate. In the Mediterranean region, evaporation plays a significant role in reservoir water budgets. Therefore, estimating water surface evaporation is essential for efficient reservoir water management. This study aims to (i) assess the reservoir evaporation pattern in southern Portugal from meteorological offshore measures, (ii) benchmark various indirect methods for evaluating reservoir evaporation at a monthly scale, and (iii) provide recommendations on the most suitable indirect method to apply in operational practices. This study presents meteorological data collected from floating weather stations on instrumented platforms across nine reservoirs in Alentejo and Algarve. This is the first time that so many offshore local measurements have been made available in a Mediterranean climate region. The reservoir evaporation was estimated by the Energy Budget (Bowen Ratio) method, having concluded that monthly evaporation rates across the nine reservoirs ranged from 0.8 mm $d^{-1}$ in winter to 4.6 mm $d^{-1}$ in summer, with an annual average of 2.7 mm $d^{-1}$. Annual evaporation values ranged from 750 to 1230 mm, showing a positive gradient from the northern Alentejo region to the southwest Algarve region. To evaluate the performance of five empirical and semi-empirical evaporation indirect methods, a benchmarking analysis was conducted. The indirect methods studied are Mass Transfer (MT), Penman (PEN), Priestley and Taylor (PT), Thornthwaite (THOR), and Pan Evaporation (PE). Regarding the MT method, an N function of a reservoir superficial area is presented for the Mediterranean climate regions. In the Pan Evaporation method, the pan coefficient was considered equal to one. The benchmarking analysis revealed that all studied methods produced estimates that had good correlation with the Energy Budget method's results across all reservoirs. All the methods showed small biases at the monthly scale, particularly in the dry semester. The estimates' evaporation variability depended on the reservoir. Overall, the evaluation of evaporation methods concluded that (i) the stakeholders should considerer having an evaporation pan offshore; (ii) to manage the water balance of the studied reservoirs, the manager must apply the method with the best performance, depending on the data available; (iii) to manage other reservoirs located in the Mediterranean climate region, the manager must compare reservoir characteristics and the data available in order to choose the most suitable method to apply.

**Keywords:** Mediterranean region; reservoirs; offshore measurements on floating platforms; evaporation; benchmarking analysis



Academic Editor: Jorge Lorenzo-Lacruz

Received: 11 September 2025
Revised: 14 October 2025
Accepted: 22 October 2025
Published: 31 October 2025
Corrected: 12 December 2025

**Citation:** Rodrigues, C.M.; Guimarães, R.C.; Moreira, M. Estimating Reservoir Evaporation Under Mediterranean Climate Using Indirect Methods: A Case Study in Southern Portugal. *Hydrology* **2025**, *12*, 286. https://doi.org/10.3390/hydrology12110286

## 1. Introduction

The Mediterranean climate is characterized by its accentuated inter-annual variability with hot and dry summers and mild and rainy winters. Moreover, the Mediterranean region is considered one of the world's hot spots of climate change. At the end of this century, climate models project an increase in air temperature (ranging between 2.2 and 5.1 °C), a decrease in rainfall (ranging between 4% and 27%), and an increase in drought periods [1]. Consequently, climate change impacts on the Mediterranean region will particularly affect the availability of water resources.

In Alentejo and Algarve, in southern Portugal, where a Mediterranean climate prevails, the availability of water relies on man-made infrastructures, such as dams and reservoirs, which are strategic elements for securing urban and industrial water supply, irrigation, and energy generation due to the challenges presented by water scarcity in this region [2–5]. However, the construction of reservoirs alters the water balance of the region and increases the loss of water resources to the atmosphere through evaporation. Evaporation from an open water body, also known as lake evaporation and referred to as reservoir evaporation throughout this paper, is one of the most important components of the water balance. According to statistics, the annual evaporation losses of the reservoirs in arid and semiarid regions account for about 40% of the total usage volume [6].

Classical studies estimating evaporation can use different approaches, including aerodynamic mass transfer formulations, energy balance formulations, or a combination of both. Based on these approaches, various methods have been developed for quantifying evaporation in reservoirs, which are classified according to theoretical developments, as discussed by [7]: (1) water balance applied to the water body, (2) energy balance applied to the water body in the reservoir, (3) aerodynamic functions (mass transfer), (4) hybrid with energy balance and aerodynamic, (5) thermic as a function of the temperature, and (6) direct measurements. Most of these methods have significant limitations. Methods based on energy balance depend on energy sources that can be solar radiation, atmospheric radiation, the sensible heat of the overlying air layer, and/or energy stored in the water body. All the methods require site-specific measurements of several meteorological variables, such as air/water temperature, humidity, wind speed, and/or solar radiation, that are not commonly available at the reservoir's water surface [8,9].

This paper presents and discusses six of these methods. The conservation energy law accounts for incoming and outgoing energy, which are balanced by the amount of energy stored in the system.

The energy balance herein considered can be expressed as

$$Q_n - \Delta Q = H + \lambda E + Q_F + Q_P \quad (1)$$

where $Q_n$ is the net radiation, $\Delta Q$ is the heat storage change in the water body, $H$ is the sensible heat flux, $\lambda E$ is the latent heat flux, $Q_F$ is the net heat flux carried by surface water and groundwater and, $Q_P$ is the net heat flux resulting from precipitation. All fluxes are in units of W m$^{-2}$.

The last two terms of Equation (1) are usually neglected because of their relatively small magnitudes compared to the other terms in the balance [10–12]. Consequently, the energy balance equation can be simplified:

$$Q_n - \Delta Q = H + \lambda E \quad (2)$$

One of many approaches is the relation between the flux of sensible heat ($H$) and the latent heat flux ($\lambda E$) through the Bowen ratio ($\beta$) (Table 1) [13,14]. Although some limitations have been identified in previous research [8,15–17], the Bowen Ratio Energy

Budget (BREB) method has been applied and selected as the reference. This method is generally regarded as one of the most robust and accurate techniques for determining evaporation [8,18–20]. BREB-derived evaporation estimates are typically within 10% of true values when averaged over a season and within 15% when averaged over a month [8,21].

**Table 1.** Mathematic formulation of the methods used in the study.

| Method | Ref. | Eq.n. | Equation | Equation Terms and Parameters |
|---|---|---|---|---|
| **BREB** | [13,14] | (3) | $E = \frac{Q_n - \Delta Q}{\rho_w[\lambda(1+\beta)+C_{pw}T_s]}(86.4 \times 10^6)$ | $Q_n = Q_s(1-\alpha) + Q_a(1-\alpha_l) - Q_{ls}$<br>$\alpha = 0.08 + 0.02\sin\left(\frac{2\pi JD}{365} + \frac{\pi}{2}\right)$<br>$Q_{ls} = \varepsilon_w \sigma (T_s + 273.15)^4$<br>$\Delta Q = \frac{\rho_w C_{pw}}{\Delta t A_L(t)} \sum \Delta T_i h_i A_i$<br>$\lambda = [2.501 - (2.361 \times 10^{-3})T_s] \times 10^6$<br>$\beta = \frac{H}{\lambda E} = \gamma\left(\frac{T_s - T_a}{e_s - e_a}\right)$<br>$H = C_p P (T_s - T_a)$<br>$\lambda E = \lambda \varepsilon (e_s - e_a)$<br>$\gamma = \frac{C_p P}{\varepsilon \lambda}$<br>$N = f(A_s)$<br>$e_s = 610.8 \exp\left(\frac{17.27 T_s}{T_s + 237.3}\right)$<br>$e_a = \frac{e_s}{HR} \times 100$<br>$e_a^* = 610.8 \exp\left(\frac{17.27 T_a}{T_a + 237.3}\right)$<br>$\Delta = \frac{4098 \times e_a^*}{(T_a + 237.3)^2}$ |
| **MT** | [7,15,18] | (4) | $E = NU_2 \times (e_s - e_a)$ | |
| **PEN** | [22,23] | (5) | $E = \frac{\Delta}{\Delta+\gamma}\frac{Q_n - \Delta Q}{\lambda \rho_w}(86.4 \times 10^6) + \frac{\gamma}{\Delta+\gamma} \times [0.26(0.5 + 0.54U_2)(e_a^* - e_a) \times 10^{-2}]$ | |
| **PT** | [24,25] | (6) | $E = \alpha_{PT}\frac{\Delta}{\Delta+\gamma}\frac{Q_n - \Delta Q}{\lambda \rho_w}(86.4 \times 10^6)$ | |
| **THOR** | [26–28] | (7) | $E = \left[1.6 \times N_m \left(\frac{10 T_{am}}{I}\right)^b\right]\left(\frac{10}{N_d}\right)$ | $N_m = \frac{n_d}{12} \times \frac{N_d}{30}$<br>$I = \sum\left(\frac{T_{am}}{5}\right)^{1.514}$<br>$b = 6.75 \times 10^{-7} I^3 - 7.71 \times 10^{-5} I^2 + 1.79 \times 10^{-2} I + 0.49$ |
| **PE** | [7,29] | (8) | $E = K_{pan} E_{pan}$ | |

The multipliers of $86.4 \times 10^6$ that appear in equations are used to convert results into mm $d^{-1}$. $E$—Reservoir evaporation rate (mm $d^{-1}$); $Q_n$—Net radiation (W $m^{-2}$); $Q_s$—Incoming solar radiation (W $m^{-2}$); $\alpha$—Surface short-wave albedo; $JD$—Julian day; $Q_a$—Incoming atmospheric radiation (W $m^{-2}$); $\alpha_1$—Surface long-wave albedo = 0.03; $Q_{ls}$—Emitting long-wave radiation from the surface (W $m^{-2}$); $\varepsilon_w$—Water emissivity = 0.97; $\sigma$—Stefan–Boltzmann constant = $5.67 \times 10^{-8}$ (W $m^{-2} K^{-4}$); $T_s$—Water surface temperature (°C); $\Delta Q$—Heat storage change in the water body (W $m^{-2}$); $\rho_w$—Density of water = 998 (kg $m^{-3}$ at 20° C); $C_{pw}$—Specific heat capacity of water = 4186 (J $kg^{-1}$ °$C^{-1}$); $\Delta t$—Time interval (s); $A_L(t)$—Reservoir surface area, a function of reservoir surface elevation and the time ($km^2$); $i$—Number of layers (1 to 5) where water temperature was measured; $\Delta T$—Temperature difference of layer $i$ in two consecutive days (°C); $h_i$—Thickness of each horizontal layer (m); $A_i$—Average area of each horizontal layer ($km^2$); $\beta$—Bowen ratio; $H$—Sensible heat flux (W $m^{-2}$); $\lambda E$—Latent heat flux (W $m^{-2}$); $\gamma$—Psychrometric constant (Pa °$C^{-1}$); $C_p$—Specific heat capacity at constant pressure = 1006 (J $kg^{-1}$ °$C^{-1}$); $P$—Atmospheric pressure (Pa); $\varepsilon$—Ratio of molecular weight of water vapor/dry air = 0.622; $\lambda$—Latent heat of

vaporization (J $kg^{-1}$); $T_a$—Air temperature (°C); $e_s$—Saturated vapor pressure at water temperature (Pa); $e_a$—Actual vapor pressure (Pa); RH—Air relative humidity (%); $N$—Mass transfer coefficient ((mm $d^{-1}$/(Pa m $s^{-1}$)); $A_s$—Water surface area ($km^2$); $U_2$—Wind speed at 2 m above the water surface (m $s^{-1}$); Δ—Slope of the saturated vapor pressure-temperature curve at mean air temperature (Pa $°C^{-1}$); $e_a^*$—Saturated vapour pressure at air temperature (Pa); $\alpha_{PT}$—Dimensionless proportionality Priestley–Taylor coefficient = 1.26; $N_m$—Correction factor according to the latitude and time of the year; $n_d$—Duration of average monthly or daily daylight (h); $N_d$—Number of days in the month; $T_{am}$—Mean monthly air temperature (°C); $I$—Annual thermal index; $b$—Polynomial function of the index; $E_{pan}$—Measured pan evaporation rate (mm $d^{-1}$), $K_{pan}$—Pan coefficient.

The Mass Transfer method (MT) (Table 1) [22,30] is one of the most widely used approaches for estimating open water evaporation due to its simplicity and reasonable accuracy. The input variables are wind speed and the difference of vapor pressure between actual and saturated vapor pressure [31]. This method assumes that the evaporation rates are a linear function of the wind speed at 2 m above the water surface, the difference between the vapor pressure at the water surface and the atmosphere, and the empirical mass transfer coefficient. The mass transfer coefficient, $N$, is usually site-dependent on various factors such as the lake shape, location and height of meteorological measurements, and climatic conditions [15]. An example of an equation to calculate $N$ as a function of surface area is $N = 0.00144A_s^{-0.050}$ for the Lake Mirror, Lake Hefner, Lake Mead and Lake Vergoritis reservoirs ([15,18,32]).

Penman [22,33] developed a combined approach of the Mass Transfer and Energy Budget methods that eliminated the need for water surface temperature in estimating open water evaporation. The Penman equation (Table 1) consists of two terms, which are commonly referred as the "energy term" and the "aerodynamic term". The first term represents the minimum possible evaporation rate, which is also known as the "equilibrium rate". The second term accounts for the influence of wind on evaporation through a wind function and the drying capacity of the atmosphere. The success of the Penman equation (PEN) in various locations is due to its solid physical foundation because it combines the Mass Transfer and Energy Budget methods [34].

Priestley and Taylor [24] proposed a simpler version of Penman's equation by considering evaporation as a function of the energy term only, as they believed the aerodynamic term could be approximated as a fixed fraction of the total evaporation. Suggesting that the aerodynamic term contributes 21% of the total evaporation, then an empirically derived parameter, $\alpha_{PT}$, with an averaged value of 1.26, was introduced for the energy component [35]. The Priestley–Taylor equation (PT) (Table 1) does not require wind speed data or the determination of the wind function for its application. Ref. [25] formulated the PT method as a truncated version of the Penman equation, where the aerodynamic component was dropped, but a coefficient greater than 1.0 is included as a multiplier.

The Thornthwaite method (THOR) (Table 1) [26] is a widely used method for estimating monthly potential evapotranspiration. This method correlates mean monthly temperature with evapotranspiration, which is determined from the water balance for valleys with sufficient moisture to maintain active transpiration [36]. Ref. [37] provided estimates of lake evaporation using the THOR formula and compared them with estimates from other models, concluding that lake evaporation was underestimated by approximately 20% relative to the other models.

The most used evaporation method is the standard pan evaporation (PE) approach (Table 1) [29,38,39]. Pan evaporation (measured US class A pan evaporation) has been widely used to monitor reservoir evaporation operationally [40–42] and in lake modeling studies [43]. Commonly, a reduction coefficient is applied to minimize the "oasis effect" caused by the advective heat and account for the large quantities of energy received through the base and sides of the pan. In lake studies [34,44], a value of 0.7 for the annual pan coefficient is usually used. However, several authors [45,46] state that pan coefficients vary

throughout the year and should be calculated for each month individually. While many studies have identified the limitations of this approach [46–49], it remains widely used as a source for large-scale validations due to its simplicity and moderate data requirements [41]. Recently, an interesting study was developed to estimate evaporative losses from reservoirs by subtracting the actual natural evapotranspiration that would have occurred on land from the evaporation caused by the flooded surface [50]. Re-analyzed climate data have also been used. Ref. [51] developed linear models (LMs) and random forest models (RFMs) to estimate reservoir evaporation in the Czech Republic.

The direct method has been applied, but, taking into account the great cost of the equipment, it is applied punctually for research aims. As an example, eddy covariance was applied to calculate Alqueva reservoir evaporation, allowing the definition of a pan coefficient for each month [42].

Ref. [52] presents a holistic overview of basin water balance, emphasizing reservoir evaporation as a topic of great relevance to researchers, consulting hydrologists, and practicing engineers. The authors highlight several issues associated with traditional methods, particularly the influence of water body heat storage on surface energy fluxes, which is rarely well quantified [52,53].

To overcome the limitations mentioned above, this study was based on data collected from floating weather stations on instrumented platforms across nine reservoirs in Alentejo and Algarve for the period 2002–2006. The complementary water temperature profile measurements are collected at the floating platforms, too. This dataset allows researchers to estimate reservoir evaporation at nine reservoirs by the energy balance method, find parameters to apply, and then compare the results of easier to apply and less demanding data-indirect methods [8,54,55], as Mass Transfer (MT), Penman (PEN), Priestley and Taylor (PT), Thornthwaite (THOR), and Pan Evaporation (PE). The results of the energy balance analysis allow for the characterization of reservoir evaporation patterns in southern Portugal. In most reservoirs, the available datasets are limited, and managers require a better understanding of reservoir evaporation. The findings of this study can be applied to other locations with similar climatic conditions. For each specific case, reservoir managers can identify the most appropriate indirect model for assessing evaporative losses and develop recommendations for operational practices in Mediterranean climate regions.

The paper is organized as follows: Section 1 presented the reservoir evaporation processes and most common methods along with the data source and objectives of this research. Section 2 describes the study area, the floating stations built in the reservoirs, the dataset and the statistic descriptors to evaluate the performance of indirect methods in relation to the estimation reservoir evaporation obtained by the energy balance and offshore measures. The pattern of reservoir evaporation in southern Portugal, and the results of the monthly benchmarking results, are presented and discussed in Section 3. Finally, Section 4 summarizes the major conclusions.

## 2. Materials and Methods

### *2.1. Study Area*

Alentejo and Algarve, located in southern Portugal (Figure 1), have a Mediterranean climate of type Csa, according to the Köppen classification. This corresponds to a temperate climate with hot, dry summers (IPMA, https://www.ipma.pt/en/oclima/normais.clima/, last accessed: 21 March 2025), and this type of climate can be found throughout the Mediterranean basin [1] and some regions of Australia and California (USA).

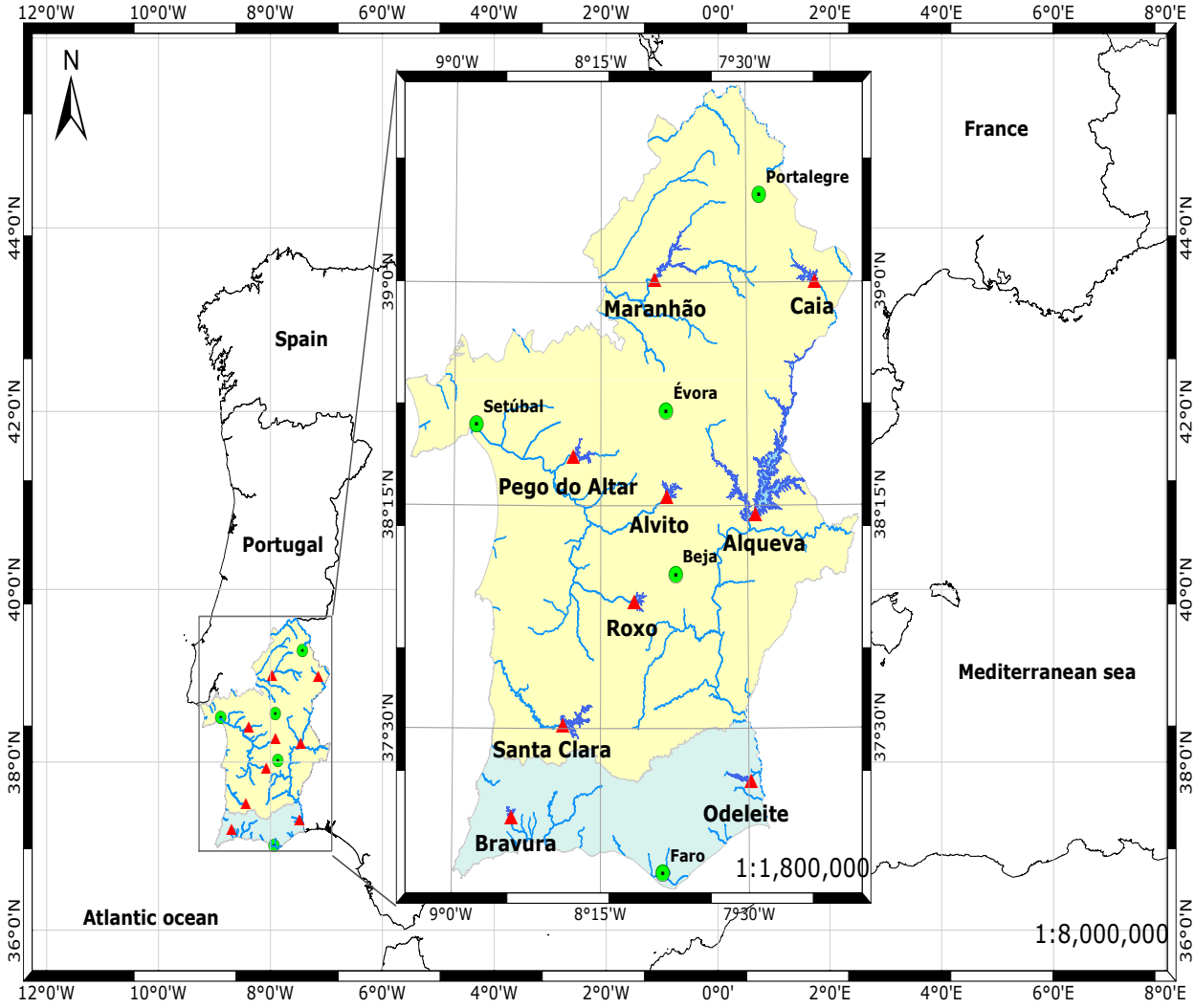


**Figure 1.** Study area location. A zoom from Alentejo (yellow) and Algarve (blue). The red triangles represent the locations of the nine monitored reservoirs, while the green circle indicates the location of the IPMA meteorological stations.

Based on the climatological normal of 1981–2010 (Instituto Português do Mar e da Atmosfera, IPMA, https://www.ipma.pt/en/oclima/normais.clima/1991-2020/#535, last accessed: 4 October 2025), the warmest months in southern Portugal are July and August with average temperatures ranging between 23.2 °C in Setúbal and 25.0 °C in Beja. In Faro (on the coast), the average maximum temperatures is the lowest, 24.5 °C, and in Beja and Évora (inland), it is the highest, 33.5 °C, while on extreme days, temperatures can exceed 45 °C in the interior of Alentejo. The coldest months are January and February with average temperatures ranging between 8.6 °C in Portalegre and 12.3 °C in Faro. During these months, average minimum temperatures vary between 4.5 °C in Évora and 8.3 °C in Faro, and negative temperatures may occur, especially in regions far away from the coastline. The average annual total rainfall varies between 455.1 mm in Faro and 838.5 mm in Portalegre, with the rainiest months being November and December, with monthly values of 75.9 mm in Évora and 124.5 mm in Portalegre.

Nine reservoirs were selected across the region (Figure 1), and the main morphometric characteristics are presented in Table 2. Reservoirs are mainly used for irrigation and domestic water supply, resulting in significant fluctuations in water levels during the dry season as large volumes of water are mobilized to meet these needs.

**Table 2.** Main reservoir morphometric characteristics.

| Parameter | Reservoirs | | | | | | | | |
|---|---|---|---|---|---|---|---|---|---|
| | **Alqueva** | **Alvito** | **Bravura** | **Caia** | **Maranhão** | **Odeleite** | **Pego do Altar** | **Roxo** | **Sta Clara** |
| NWL (m) | 152.0 | 197.5 | 84.1 | 233.5 | 130.0 | 52.0 | 52.3 | 136.0 | 130.0 |
| V ($hm^3$) | 4150.0 | 132.5 | 34.8 | 192.3 | 205.4 | 130.0 | 94.0 | 96.3 | 485.0 |
| $A_s$ ($km^2$) | 250.0 | 14.8 | 2.9 | 19.7 | 19.6 | 7.2 | 8.0 | 13.8 | 19.9 |
| Mn depth (m) | 16.6 | 8.9 | 12.2 | 9.8 | 10.5 | 18.1 | 11.8 | 7.0 | 24.4 |
| Mx depth (m) | 77.0 | 32.8 | 34.5 | 37.2 | 44.0 | 41.3 | 37.3 | 27.3 | 71.6 |
| P(km) | 1160.0 | 93.2 | 33.9 | 99.8 | 188.0 | 65.3 | 94.7 | 99.2 | 230.0 |
| L (km) | 83.0 | 7.0 | 5.5 | 12.8 | 25.0 | 18.0 | 15.0 | 4.3 | 21.2 |
| (P/L) | 14.0 | 13.3 | 6.2 | 7.8 | 7.5 | 3.6 | 6.3 | 23.1 | 10.9 |
| $K_c$ (–) | 30.3 | 6.8 | 5.6 | 6.3 | 11.9 | 6.8 | 9.4 | 7.5 | 14.5 |
| $A_d$ ($km^2$) | 55,400.0 | 212.0 | 76.8 | 571.0 | 2282.0 | 352.0 | 743.0 | 351.0 | 520.0 |
| $A_d/A_s$ | 222.0 | 14.0 | 27.0 | 29.0 | 116.0 | 49.0 | 93.0 | 25.0 | 26.0 |

NWL—Normal water level; V—Total reservoir capacity; As—Water surface area; Mn depth—Mean depth; Mx depth—Maximum depth; P—Water surface perimeter; L—Reservoir length; $K_c$—Compacity coefficient (Gravellius); $A_d$ —Catchment area.

### *2.2. Floating Stations*

A floating monitoring station was designed and built for each one of the selected reservoirs to record meteorological and water temperature data. These stations are part of the Portuguese Water Resources Monitoring Network (SNIRH, https://snirh.apambiente.pt, last accessed: 21 March 2025) and were installed over wooden floating platforms with a 30 $m^2$ area, which were anchored in place by ropes tied to three sunk concrete blocks. The meteorological station installed on each platform records pan evaporation, downward solar radiation, atmospheric pressure, precipitation, air temperature, air relative humidity, and wind speed and direction. Data are recorded at a frequency of one value per 10 min, except precipitation and wind speed, which are recorded every minute according to precipitation events. Data are used on an hourly average scale. To reduce the effects of direct solar radiation on the walls of the pan and ensure closer proximity between the temperatures of the water in the pan and in the reservoir, the pan is recessed into the platform, contacting the reservoir water. Wind speed and direction, air temperature, and relative humidity are recorded at three levels (2, 5, and 8 m), and the vertical wind speed sensor is located 2 m above the water surface on an additional rod that includes a sensor for measuring atmospheric pressure and solar panels for charging the system batteries. The water temperature in the reservoirs was also monitored continuously using five sensors placed at depths of 1, 5, 10, 15, and 20 m. These sensors were installed along a steel cable with a ballast at its lower end to keep the cable in a vertical position. To protect the probes and reduce the risk of any winding in the mooring cables of the platform, the entire assembly, including the cable and sensors, is positioned inside a perforated tube (high-density polyethylene) with a 90 mm diameter. A schematic layout and the dimensions of the floating monitoring stations are presented in Figure 2.

The floating stations were installed in 2001 with the exception of the Alqueva reservoir where the station was established in 2002. All measurements were parametrized, pre-processed, and temporarily stored in a data acquisition system, GEOLOG S (Logtronic, GmbH, Hamburg, Germany), expanded in its standard configuration to accommodate all sensors. The locally stored data were transmitted via GSM to the SNIRH central repository either daily or upon request.

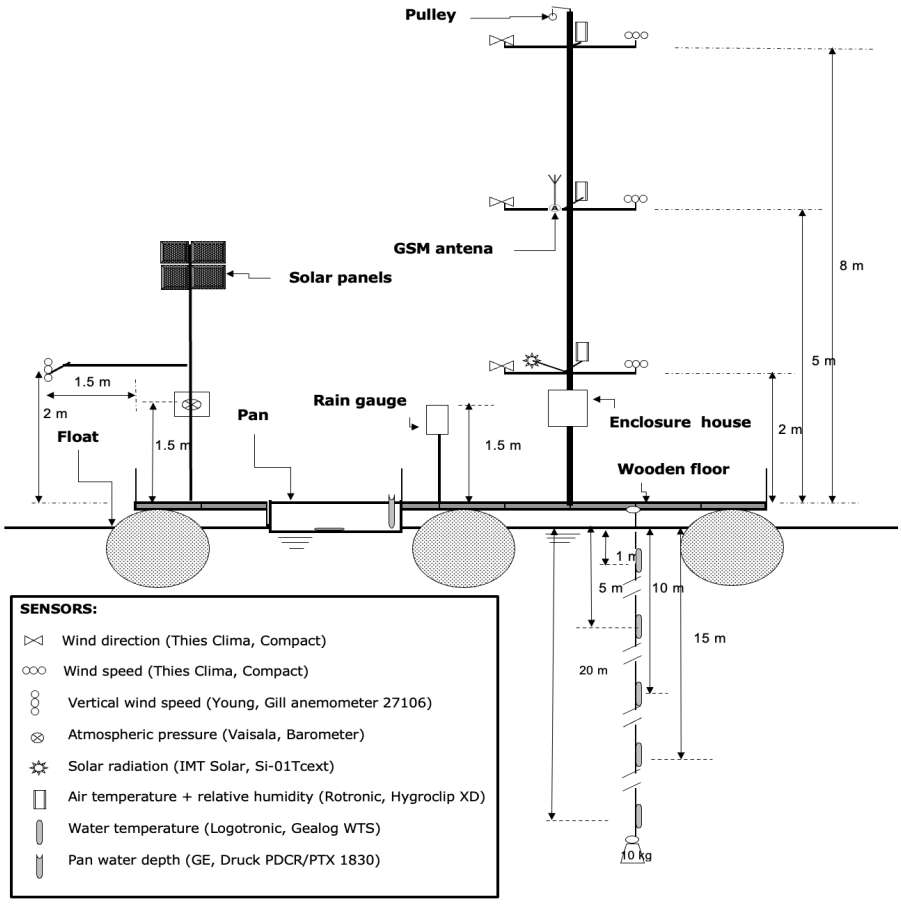


**Figure 2.** Schematic representation of meteorological and water temperature floating stations.

### *2.3. Meteorological Data and Water Body Temperature*

Meteorological and water body temperature data from the nine floating stations were recorded between 2002 and 2006 by the first author.

The annual cycle and daily data of air temperature, air relative humidity, wind speed, and solar radiation at 2 m high were characterized. Water surface temperature was also analyzed. The graphical representation of the data time series is presented at Figure 3.

The annual cycle of air temperature between the different reservoir locations shows great homogeneity, ranging from 8.5 to 24.2 ºC. During winter, the highest temperatures are observed in reservoirs located further south, particularly in Bravura, which records temperatures about 4 ºC higher than those in other reservoirs. During summer, Odeleite has higher air temperatures, while Bravura has lower air temperatures. It can be verified that the air temperature in the Bravura reservoir has the lowest amplitude and the smallest variation throughout the year, which can be attributed to its proximity to the sea. The behavior of air relative humidity is identical to that of air temperature. The recorded values fall within the expected range for the region, with the highest values (>80 %) occurring in November, December, and January, and the lowest values (<50%) occurring in the summer months. The lowest value was recorded in July, during which the variability between reservoirs was more pronounced. The Bravura reservoir exhibited the lowest amplitude, ranging from 65.7% in July to 80.3% in November. Significant differences in wind speed were observed between reservoirs. While the annual cycle in each reservoir demonstrated a smooth variation, a slight upward trend in wind speed during summer months was noted, particularly in the Bravura and Odeleite reservoirs. This increase in wind speed may be attributed to the summer breeze characteristic of southern Portugal afternoons and may explain the greater variability in wind speed values observed in these two reservoirs, whose

local physiography favors the establishment of long fetches from the north quadrant. The Maranhão and Pego do Altar reservoirs consistently exhibited the lowest wind intensity throughout the year. The behavior of incoming solar radiation is quite similar across all nine reservoirs. The annual cycle of solar radiation is consistent for most of the reservoirs with identical behavior in winter across all reservoirs. However, during summer months, higher values are observed in the Santa Clara and Bravura reservoirs, while lower values are observed in the Maranhão reservoir.

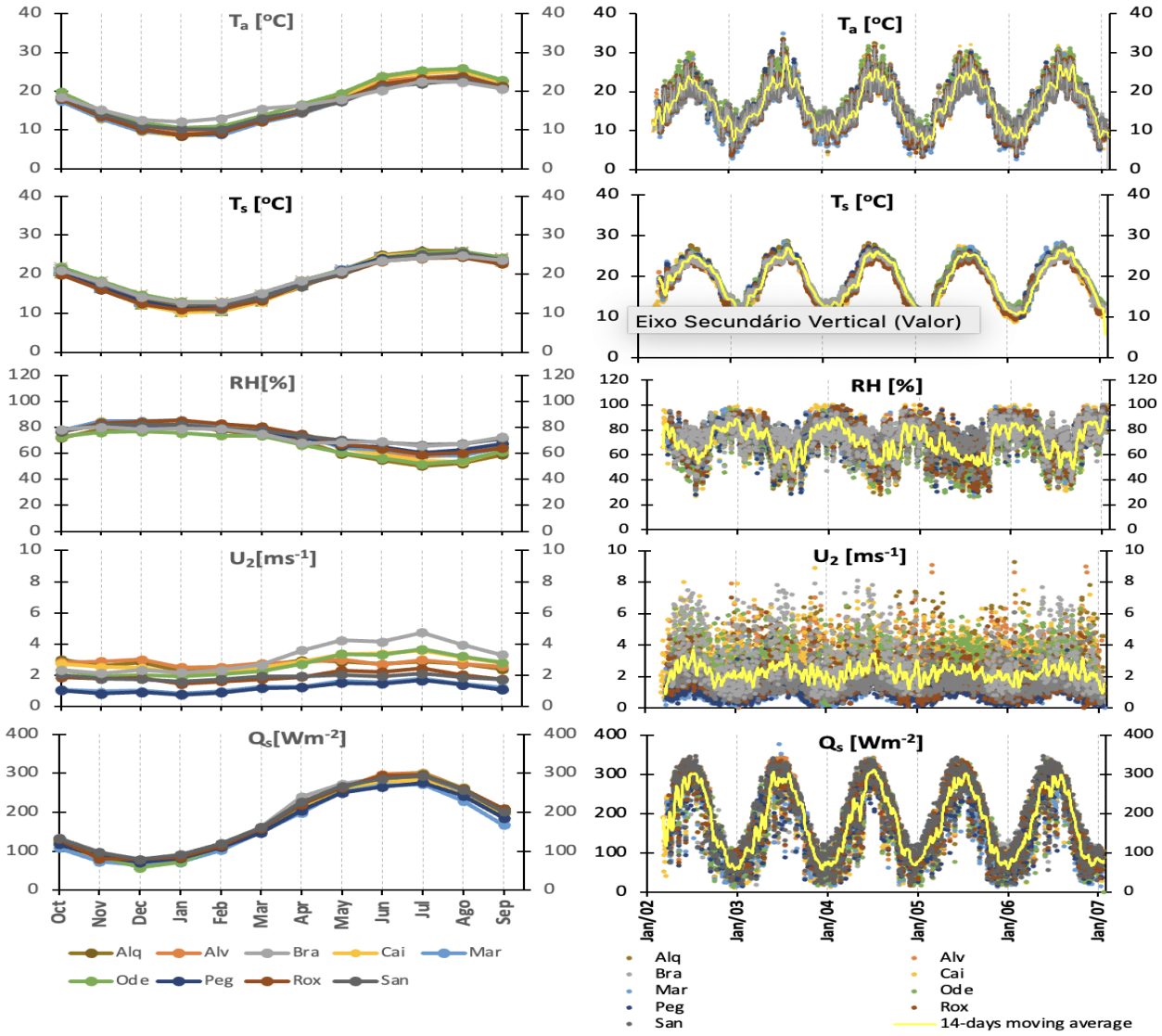


**Figure 3.** Annual cycle (**left**) and daily mean data (**right**) of air temperature ($T_a$), water surface temperature ($T_s$), air relative humidity (RH), wind speed ($U_2$) and incoming solar radiation ($Q_s$) measured at 2 m high. The 14 days forward–moving average was obtained considering the data from all reservoirs.

Figure 4 presents daily water temperatures ($T_w$) recorded at depths of 1, 5, 10, 15, and 20 m in the reservoirs. A spatial and temporal analysis of water temperature reveals consistent thermal behavior between reservoirs, with the greatest amplitudes occurring at the surface, ranging 16–18 °C. The highest water surface temperatures range 25–27 °C and are observed in July and August. At the maximum monitored depth (20 m), recorded water temperature amplitudes varied 8–10 °C. Minimum values were observed in January and February with most reservoirs recording values not falling below 10 °C.

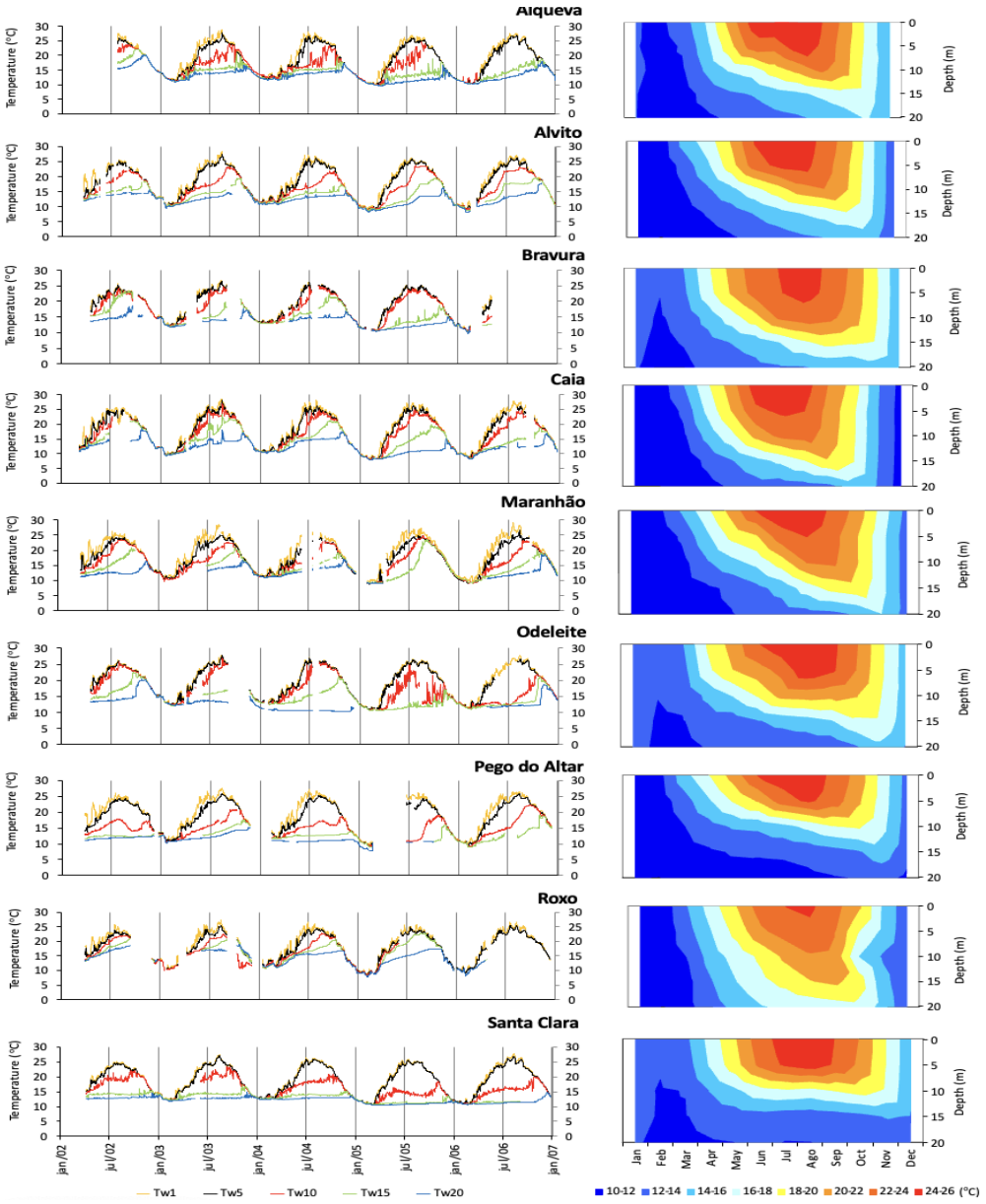


**Figure 4.** Daily mean water temperature observed at 1 ($T_w1$), 5 ($T_w5$), 10 ($T_w10$), 15 ($T_w15$) and 20 ($T_w20$) meters depth in the reservoirs (**on left**) and corresponding annual cycle (**on right**). The gaps in the graphics indicate periods of missing data resulting from equipment failures.

The temperature profiles exhibit a consistent annual cycle across most reservoirs. In January, all reservoirs display an isothermal profile. As air temperature, solar radiation, and day length increase in April, the water column experiences deep heating, leading to thermal stratification that reaches its peak during summer. By June, some reservoirs exhibit an upper-mixed layer, which is characterized by constant temperature (upper-mixed layer induced by surface agitation) overlapping a layer where the temperature varies with depth (thermocline). As autumn begins, the surface temperature gradually decreases, extending to deeper layers and leading to a progressive reduction in the thermocline until the isothermal profile is re-established in January or February.

### *2.4. Methods Performance Evaluators*

The performance of the indirect methods was evaluated using the statistical descriptors [7] presented in Table 3. The Index of Performance, $d$, was classified according to Table 4 [56].

**Table 3.** Statistical descriptors.

| Descriptor | Eq.n. | Equation | Range | Optimum Value |
|---|---|---|---|---|
| **Root mean square error** | (9) | $RMSE = \sqrt{\frac{1}{n}\sum_{i=1}^{n}(S_i - O_i)^2}$ | 0 to $+\infty$ | 0 |
| **Correlation coefficient** | (10) | $R = \frac{1}{n}\sum_{i=1}^{n}\frac{(S_i-\overline{S})(O_i-\overline{O})}{\sigma_S\sigma_O}$ | $-1$ to 1 | 1 |
| **Index of agreement** | (11) | $IoA = 1 - \left[\frac{\sum_{i=1}^{n}(S_i-O_i)^2}{\sum_{i=1}^{n}(\lvert S_i-\overline{S}\rvert+\lvert O_i-\overline{O}\rvert)^2}\right]$ | 0 to 1 | 1 |
| **Index of performance** | (12) | $d = R \times IoA$ | 0 to 1 | 1 |

$S_i$—Indirect method values; $O_i$—BREB values; $\overline{S}$—Mean of the indirect method values; $\sigma_S$—Standard deviation of the indirect method values; $\overline{O}$—Mean of the BREB values; $\sigma_O$—Standard deviation of the BREB values; $n$—Number of values.

**Table 4.** Classification of Index of performance, *d* [7].

| Index of Performance, *d* | Performance |
|---|---|
| >0.85 | *Excellent* |
| 0.76–0.85 | *Very good* |
| 0.66–0.75 | *Good* |
| 0.61–0.65 | *Average* |
| 0.51–0.60 | *Poor* |
| 0.41–0.50 | *Bad* |
| <0.40 | *Very bad* |

## 3. Results and Discussion

### *3.1. Patterns of Reservoir Evaporation in Southern Portugal*

Considering the energy balance, Table 5 shows the annual mean energy fluxes for the nine reservoirs. In the absence of on-site atmospheric radiation ($Q_a$) measurements, the European Centre for Medium-Range Weather Forecasts (ECMWF) analysis was used (http://www.ecmwf.int/products/forecasts/d/charts, last accessed: 21 March 2025). The energy balance closure (EBC) was calculated by

$$EBC(\%) = \left(\frac{H + \lambda E}{Q_n - \Delta Q} - 1\right) \times 100 \quad (13)$$

For most reservoirs, the heat storage change ($\Delta Q$) is close to zero, confirming that the net heat flux carried by surface water and groundwater ($Q_F$) and the net heat flux resulting from precipitation ($Q_P$) can be neglected. The *EBC* shows good results for almost reservoirs except for Bravura, Caia, and Maranhão. Comparing Bravura and Odeleite, despite Bravura being located under a more Atlantic influence with a different wind pattern and a smaller surface area, the latent heat flux can be overestimated. For the Caia and Maranhão reservoirs, which are located at higher latitudes, the incoming atmospheric radiation may be underestimated when compared to Pego do Altar, which lies further inland at a much higher altitude. These findings allow us to conclude that even for these reservoirs, the net heat flux carried by the surface water and groundwater ($Q_F$) and the net heat flux resulting from precipitation ($Q_P$) can be neglected.

The monthly values for the different components of the heat budget, including net radiation, latent heat, sensible heat, and heat storage change, are illustrated in Figure 5.

**Table 5.** Annual mean values of reservoir energy fluxes (W $m^{-2}$) and the *EBC* (%).

| | Reservoirs | | | | | | | | |
|---|---|---|---|---|---|---|---|---|---|
| | **Alqueva** | **Alvito** | **Bravura** | **Caia** | **Maranhão** | **Odeleite** | **Pego do Altar** | **Roxo** | **Sta Clara** |
| $Q_a(1-\alpha_1)$ | 314.2 | 317.0 | 320.5 | 310.3 | 313.6 | 316.4 | 315.9 | 317.0 | 320.5 |
| $Q_{ls}$ | 402.1 | 399.2 | 402.2 | 399.1 | 399.7 | 404.1 | 400.6 | 399.0 | 402.4 |
| *LW Balance* | −87.9 | −82.2 | −81.7 | −88.8 | −86.1 | −87.7 | −84.7 | −82.0 | −81.9 |
| $Q_s(1-\alpha)$ | 162.6 | 169.9 | 173.5 | 161.8 | 154.0 | 168.0 | 159.0 | 169.4 | 173.4 |
| $Q_n$ | 74.7 | 87.7 | 91.8 | 73.0 | 67.9 | 80.3 | 74.3 | 87.4 | 91.5 |
| $\Delta Q$ | −0.2 | 0.1 | 0.4 | 0.2 | 1.9 | −0.8 | 0.6 | −1.2 | −0.9 |
| $\lambda E$ | 74.4 | 76.7 | 96.6 | 79.4 | 74.6 | 77.9 | 65.3 | 79.9 | 79.0 |
| $H$ | 5.4 | 8.3 | 6.8 | 6.8 | 8.0 | 4.2 | 7.1 | 10.2 | 12.5 |
| *EBC* | 6.5 | −3.0 | 13.1 | 18.4 | 25.2 | 1.2 | −1.8 | 1.7 | −1.0 |

Net loss of heat in the long-wave radiative balance, $LW$, is calculated by $LW = [Q_a(1-\alpha_1) - Q_{ls}]$.

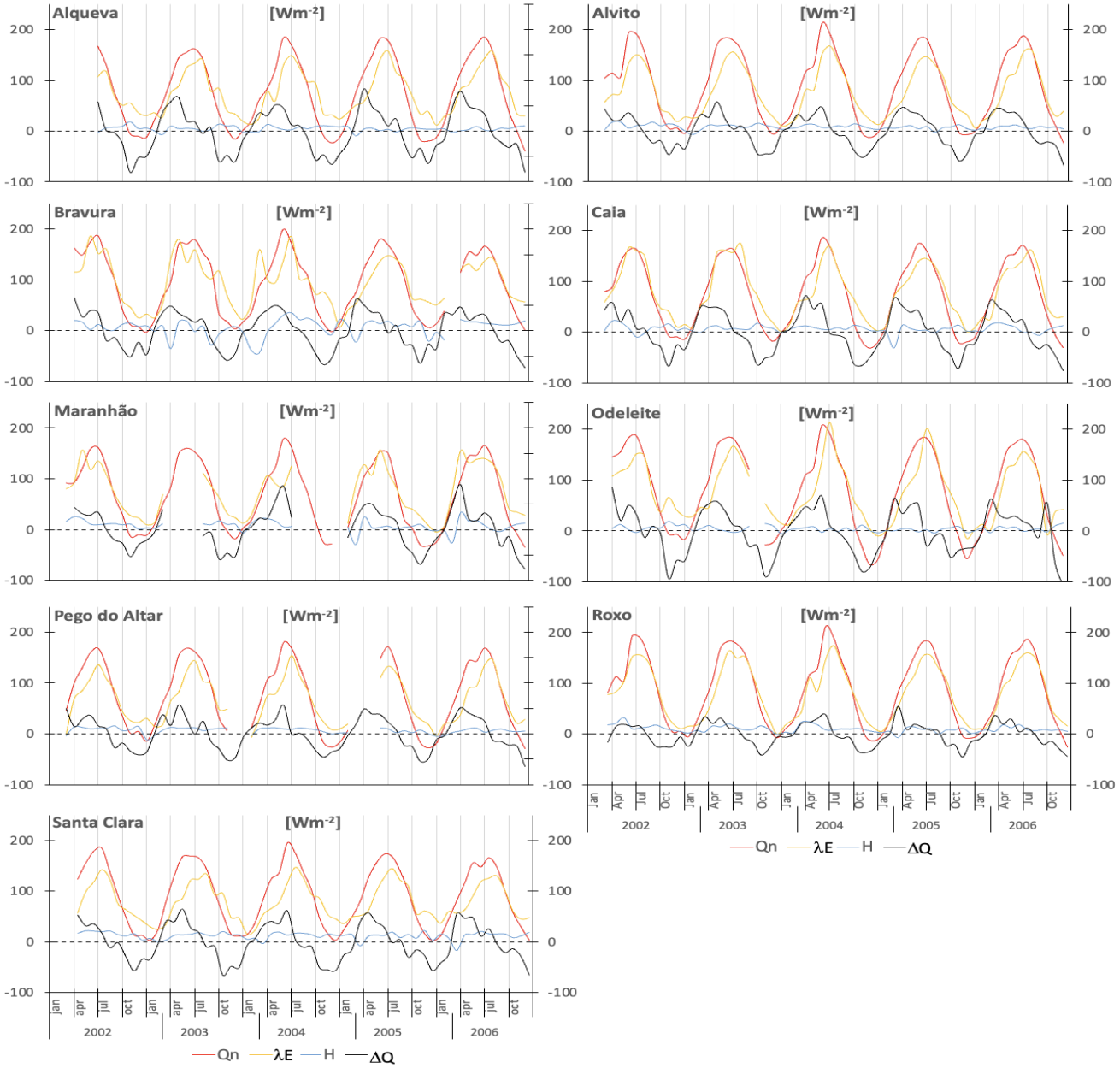


**Figure 5.** Monthly energy balance components in reservoirs. Net radiation ($Q_n$), heat storage change in the water body (ΔQ), latent heat flux, ($\lambda E$) and sensible heat flux ($H$).

The monthly variation of latent heat flux ($\lambda E$) exhibits a strong seasonality that aligns with the net radiation ($Q_n$), which is the primary energy source for the heat balance. The maximum $\lambda E$ flux typically lags the peak values of $Q_n$. On the other hand, the minimum $\lambda E$ flux is primarily influenced by the heat storage change ($\Delta Q$). In most reservoirs, the annual $\Delta Q$ approaches zero, indicating a null balance between energy gains and losses throughout the years. The energy dynamics of the reservoirs can be understood by analyzing the gains and losses of energy by the water body over the year. During spring, the reservoirs experience an energy gain and storage phase driven by net radiation and low evaporation rates. Generally, the energy begins to increase from February or March until August, reaching its maximum around April (although this timing can vary across years and reservoirs, sometimes occurring in May or June). From September onwards, the energy storage variation reverses, and the water mass undergoes an energy reduction, typically lasting until January, with the maximum energy loss occurring in November. $\Delta Q$ exhibits large positive and negative values, ranging from 55.2 to 88.8 W m$^{-2}$ and $-45.7$ to $-93.1$ W m$^{-2}$, respectively. During autumn, as solar radiation decreases, the energy required for evaporation is sourced from the release of $\Delta Q$ in the form of $\lambda E$ and, to a lesser extent, $H$. $Q_n$ fluxes display seasonal trends, with the highest values observed in summer, following a similar pattern to solar radiation ($Q_s$). However, in some winter months, negative values of $Q_n$ can be observed.

The annual mean $Q_n$ ranges from 68 to 92 W m$^{-2}$ for all reservoirs, as shown in Table 5. $H$ depends on the temperature difference between the water surface ($T_s$) and the air ($T_a$). $H$ has relatively low values compared to other components of the energy balance. It is generally positive since, on average, $T_s$ is higher than $T_a$. Under these conditions ($T_s > T_a$), the sensible heat flow occurs from the water surface to the atmosphere, resulting in energy loss from the lake.

Daily evaporation values were determined for all reservoirs using the BREB method, as described by Equation (3). The monthly evaporation is presented in Figure 6. To identify possible outliers, the annual cycles of mean, maximum, and minimum evaporation were also presented. Although there are no substantial inter-annual variations in evaporation, a pronounced seasonality is evident. The highest evaporation rates are observed from June to August, while the lowest rates occur between December and February. Generally, the monthly mean evaporation falls within the expected range for each respective month, indicating a reasonable consistency throughout the period.

When comparing the monthly evaporation rates shown in Figure 7, it is evident that July has the highest evaporation values, while January experiences the lowest rates. The maximum monthly evaporation ranges from 4.4 mm d$^{-1}$ in the Maranhão reservoir to 6.7 mm d$^{-1}$ in the Bravura reservoir. In general, the minimum monthly evaporation is nearly zero for most reservoirs, except for Alqueva and Santa Clara, which have values ranging from 0.4 to 0.6 mm d$^{-1}$, respectively. Across all reservoirs, the monthly evaporation varies from 0.8 mm d$^{-1}$ in winter to 4.0 mm d$^{-1}$ in summer with an average of 2.7 mm d$^{-1}$. These values align with other measurements in the Mediterranean region, as reported in studies by [57] or [58]. The latter authors studied the Mediterranean region of Sardinia, Italy, and concluded that evaporation ranged from 0.58 mm d$^{-1}$ in winter to 4.96 mm d$^{-1}$ in summer with an average of 2.63 mm d$^{-1}$.

Figure 8 illustrates the spatial distribution of mean seasonal reservoir evaporation values in southern Portugal. The values were obtained through inverse distance interpolation for the dry and wet semesters, respectively. Figure 9 displays the spatial distribution of mean annual reservoir evaporation values. The patterns of reservoir evaporation exhibit distinct seasonal and spatial variations. Throughout the year, a clear minimum is observed in the northern part of the region, while the maximum values are concentrated in the south-

west Algarve region. This spatial pattern is consistent in both the dry and wet semesters. The annual evaporation losses range from 750 to 1230 mm, showing a significant positive gradient from the northern part of the region toward the southwest Algarve region. This indicates that the reservoirs in the Algarve region experience higher evaporation rates compared to those in the northern areas. These differences can be explained by the higher solar radiation typically observed in the southern areas compared to the north and by the stronger wind regimes along the coastal zones, which enhance evaporation rates.

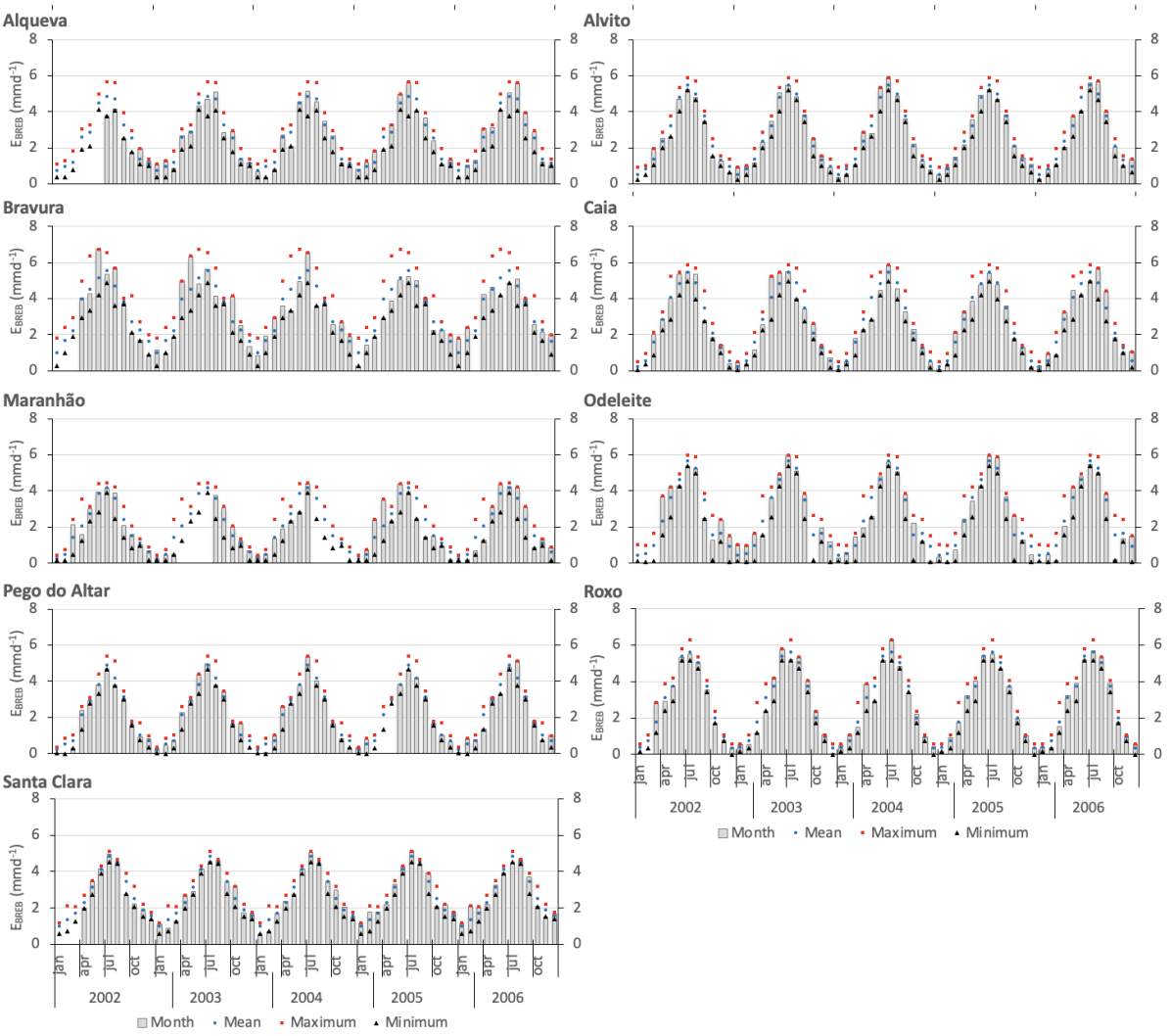


**Figure 6.** Monthly energy budget evaporation (bars) and the annual cycle of mean (circles), maximum (squares), and minimum (triangles) values.

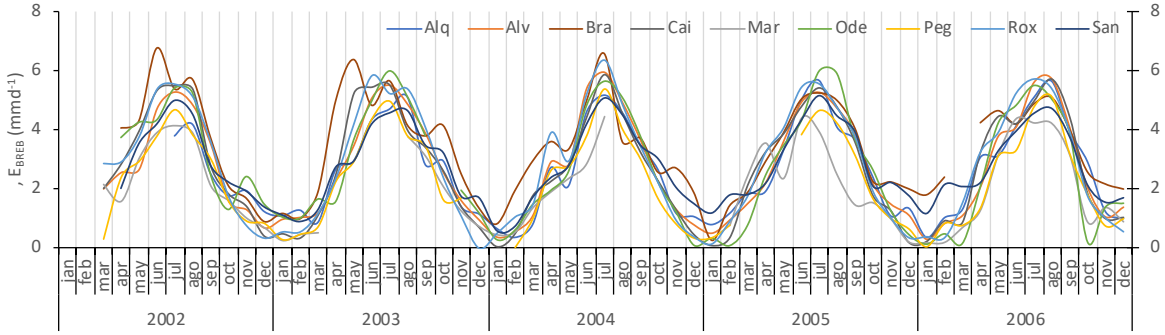


**Figure 7.** Monthly mean evaporation estimated by the BREB method.

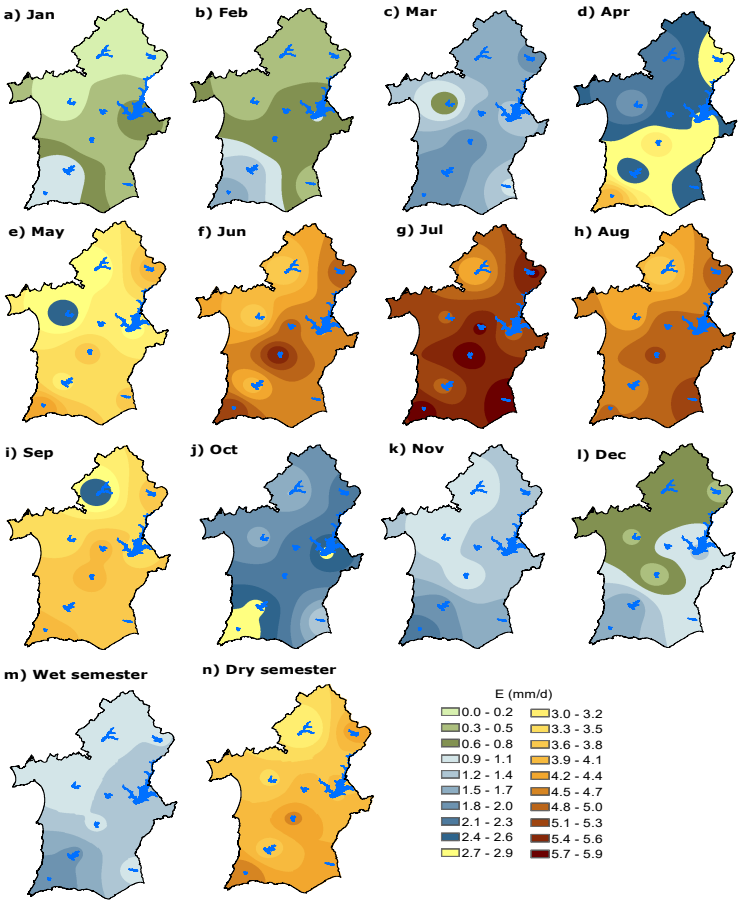


**Figure 8.** Spatial distribution of monthly mean (**a**–**l**) and seasonal mean (**m**,**n**) reservoir evaporation in southern Portugal.

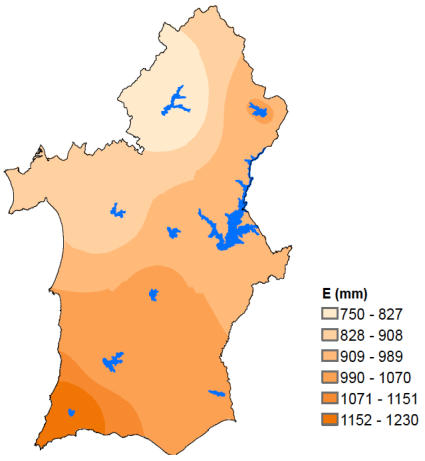


**Figure 9.** Spatial distribution of mean annual reservoir evaporation in southern Portugal.

### *3.2. Benchmarking of Indirect Methods*

Given that the measured parameters required for direct estimation are often unavailable, a monthly benchmarking analysis was conducted to evaluate the performance of different indirect methods for estimating reservoir evaporation. Five evaporation models, as summarized in Table 1, were applied to compute reservoir evaporation for the nine reservoirs included in this study.

Figure 10 illustrates the comparison between monthly evaporation estimates obtained from the five indirect methods and the evaporation estimated with the BREB method, using the Alqueva reservoir as an example. The figure displays the trend line and the 1:1 line (left)

and the differences in average monthly evaporation for both the wet and dry semesters (right). Table 6 presents the same results for all reservoirs.

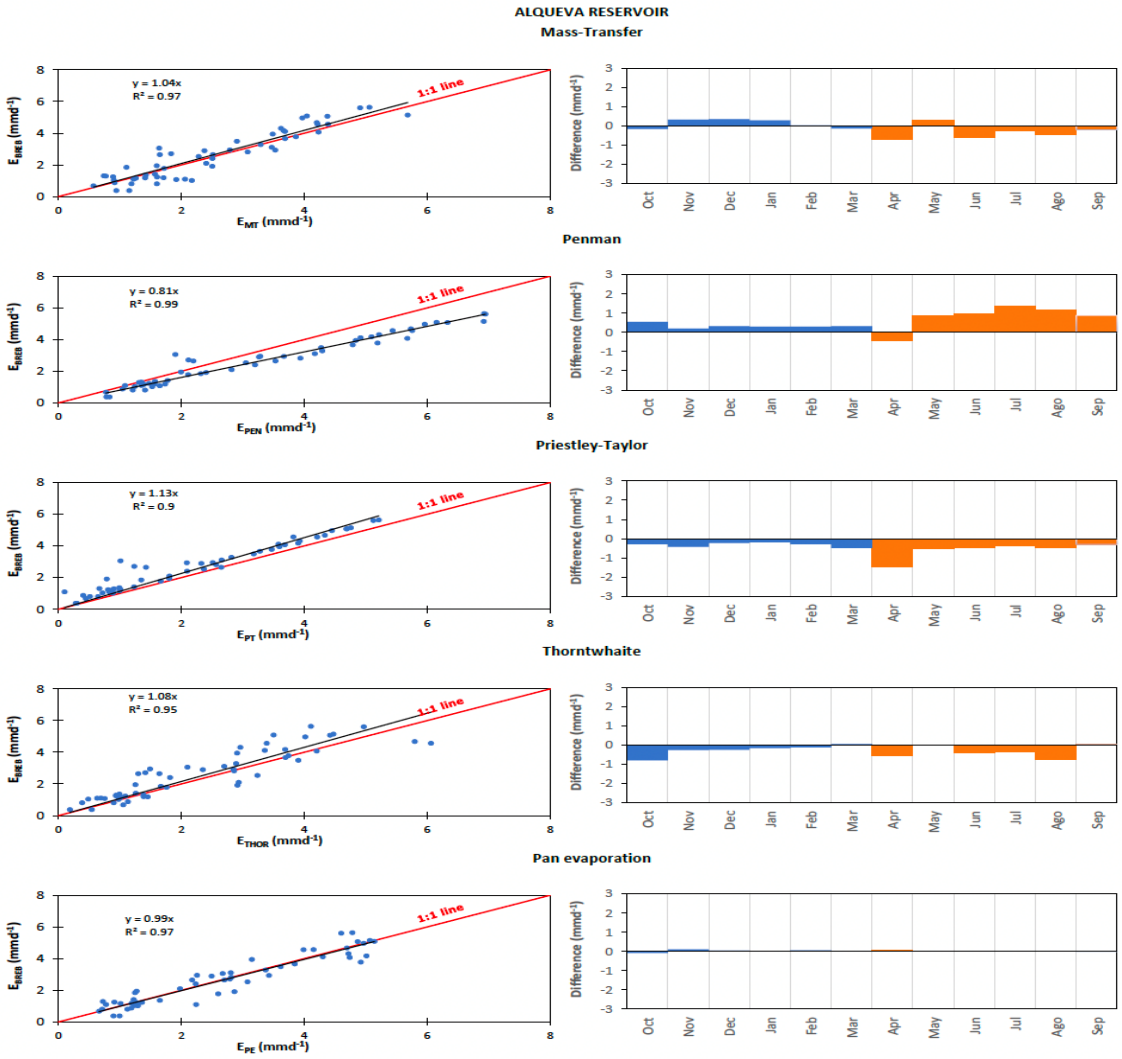


**Figure 10.** Evaporation estimated by the 5 indirect methods compared to evaporation calculated by the Energy Budget method ($E_{BREB}$) for Alqueva reservoir: **Left**—trend lines; **right**—difference for the average monthly evaporation, blue—wet semester; orange—dry semester.

Table 7 presents the estimation of the mass transfer coefficient ($N$) for each reservoir. There is a strong correlation ($R^2$) between the evaporation rates estimated by the Energy Budget method and the Mass Transfer product $U_2 \times (e_s - e_a)$. However, variations in $N$ were observed among the reservoirs, which can be attributed to differences in exposure to prevailing winds and physiographic characteristics of the water bodies. It was observed that the mass transfer coefficient decreases with an increase in the water surface area of the reservoirs, which is consistent with the findings from studies conducted on lakes in the USA (Mirror, Hefner, Mead) [15] and the Greek lake Vegoritis [59]. The calculated $N$ value for these lakes was slightly higher than the values obtained in our study, resulting in higher evaporation rate estimates for those cases. This discrepancy can be attributed to differences in measurement procedures, such as the measurement of atmospheric humidity being conducted on the shore upwind of those lakes, while in our study, all measurements were made offshore in the reservoir.

**Table 6.** Evaporation estimated by the 5 indirect methods compared to evaporation calculated by the Energy Budget method. The annual mean, determination coefficient and maximum and minimum differences in average monthly evaporation for wet and dry semesters (mm $d^{-1}$).

| Reservoir | Method | Mean | $R^2$ | MaxB_WS | MinB_WS | MaxB_DS | MinB_DS |
|---|---|---|---|---|---|---|---|
| Alqueva | MT | 2.52 | 0.97 | 0.62 | −0.06 | −0.21 | −0.04 |
| | PEN | 3.20 | 0.99 | 0.52 | 0.15 | 0.31 | −0.13 |
| | PT | 2.17 | 0.98 | −0.42 | −0.11 | −0.57 | −0.09 |
| | THOR | 2.30 | 0.95 | −0.29 | −0.04 | −0.16 | 0.03 |
| | PE | 2.60 | 0.96 | 0.35 | 0.01 | 0.06 | 0.00 |
| Alvito | MT | 2.75 | 0.98 | 0.97 | −0.01 | 0.18 | −0.01 |
| | PEN | 3.13 | 1.00 | 0.85 | 0.16 | 0.18 | 0.10 |
| | PT | 2.42 | 1.00 | −0.30 | −0.08 | −0.15 | −0.07 |
| | THOR | 2.20 | 0.98 | 0.47 | 0.01 | −0.24 | −0.16 |
| | PE | 2.72 | 0.99 | −0.16 | 0.02 | 0.02 | 0.02 |
| Bravura | MT | 3.15 | 0.86 | −0.48 | −0.20 | −0.29 | 0.03 |
| | PEN | 3.47 | 0.97 | 1.10 | 0.02 | 0.17 | 0.04 |
| | PT | 2.68 | 0.97 | −0.56 | −0.11 | −0.34 | −0.10 |
| | THOR | 2.53 | 0.94 | 0.84 | 0.08 | −0.46 | −0.07 |
| | PE | 3.12 | 0.95 | 0.92 | 0.04 | −0.45 | −0.17 |
| Caia | MT | 2.72 | 0.96 | 1.35 | 0.10 | −0.23 | 0.03 |
| | PEN | 3.07 | 0.97 | 1.27 | −0.04 | 0.28 | 0.10 |
| | PT | 2.20 | 0.97 | −0.67 | −0.09 | −0.36 | −0.10 |
| | THOR | 2.35 | 0.96 | 0.37 | 0.01 | −0.39 | −0.02 |
| | PE | 2.74 | 0.97 | 0.73 | 0.00 | 0.11 | 0.01 |
| Maranhão | MT | 2.06 | 0.97 | 2.23 | −0.07 | −0.18 | 0.02 |
| | PEN | 2.52 | 0.95 | 0.97 | −0.06 | 1.07 | 0.14 |
| | PT | 2.22 | 0.93 | −0.93 | 0.01 | 1.15 | −0.01 |
| | THOR | 2.22 | 0.93 | 2.08 | 0.38 | 0.37 | 0.04 |
| | PE | 2.54 | 0.76 | 0.45 | −0.01 | 0.65 | 0.00 |
| Odeleite | MT | 2.90 | 0.96 | 3.15 | −0.02 | 0.13 | 0.00 |
| | PEN | 3.45 | 0.99 | 1.49 | 0.11 | 0.37 | 0.23 |
| | PT | 2.32 | 0.98 | −1.33 | −0.50 | −0.23 | 0.00 |
| | THOR | 2.52 | 0.97 | 2.08 | 0.22 | −0.17 | −0.08 |
| | PE | 2.83 | 0.97 | 3.26 | 0.00 | 0.12 | 0.03 |
| Pego do Altar | MT | 2.37 | 0.96 | 1.83 | −0.01 | 0.21 | 0.00 |
| | PEN | 2.39 | 1.00 | 1.15 | 0.07 | 0.04 | −0.02 |
| | PT | 2.10 | 1.00 | −0.44 | −0.09 | −0.13 | −0.06 |
| | THOR | 2.27 | 0.97 | 1.67 | −0.01 | −0.13 | −0.01 |
| | PE | 2.30 | 0.97 | 0.85 | 0.02 | −0.20 | 0.00 |
| Roxo | MT | 2.82 | 0.97 | 1.61 | −0.22 | −0.25 | 0.00 |
| | PEN | 3.16 | 0.99 | 1.26 | −0.01 | 0.14 | 0.05 |
| | PT | 2.46 | 0.99 | −0.38 | −0.11 | −0.22 | −0.07 |
| | THOR | 2.54 | 0.97 | 0.62 | −0.21 | −0.40 | −0.01 |
| | PE | 2.89 | 0.96 | 0.29 | 0.00 | 0.06 | 0.00 |
| Santa Clara | MT | 2.71 | 0.97 | 0.23 | 0.00 | −0.09 | −0.01 |
| | PEN | 2.82 | 1.00 | −0.16 | 0.00 | 0.04 | 0.00 |
| | PT | 2.48 | 0.99 | −0.45 | −0.09 | −0.17 | −0.04 |
| | THOR | 2.04 | 0.97 | −0.39 | −0.06 | −0.35 | −0.14 |
| | PE | 2.87 | 0.95 | 1.1 | 0.03 | −0.01 | 0.03 |

MaxB_WS—Maximum bias in wet semester; Min_Bws—Minimum bias in wet semester; MaxB_DS—Maximum bias in dry semester; MinB_DS—Minimum bias in dry semester.

An overall relationship between $N$ and the reservoir water surface area ($A_s$) was established to be applied in the Mediterranean climate region:

$$N = 0.00139 A_s^{-0.049} \quad (14)$$

**Table 7.** Mass transfer coefficient, $N$ ((mm d$^{-1}$)/(Pa m s$^{-1}$)), and its relationship with water surface area, $A_S$ (km$^2$).

| Reservoirs | $A_s$ | $N$ | $R^2$ | $N = f(A_s)$ |
|---|---|---|---|---|
| **Alqueva** | 250 | 0.00092 | 0.88 | $0.00139A_s^{-0.049}$ |
| **Alvito** | 14.8 | 0.00101 | 0.91 | |
| **Bravura** | 2.85 | 0.00104 | 0.60 | |
| **Caia** | 19.7 | 0.00990 | 0.91 | |
| **Maranhão** | 19.6 | 0.00158 | 0.71 | |
| **Odeleite** | 7.2 | 0.00095 | 0.90 | |
| **Pego do Altar** | 7.98 | 0.00176 | 0.83 | |
| **Roxo** | 13.78 | 0.00157 | 0.90 | |
| **Santa Clara** | 19.86 | 0.00159 | 0.79 | |
| **Lake Mirror** | 0.15 | 0.00164 | | $0.00144A_s^{-0.050}$ |
| **Lake Hefner** | 10.5 | 0.00095 | | |
| **Lake Mead** | 640 | 0.00118 | | |
| **Lake Vergoritis** | 33.5 | 0.00143 | | |

The comparison between monthly evaporation estimated using the MT method and the evaporation estimated using the BREB method is presented in Figure 10 and Table 6. The trend lines closely follow the 1:1 line, indicating a high level of accuracy in the MT method's estimation of evaporation for all nine reservoirs. However, there is a slight underestimation observed for the largest studied reservoir (Alqueva), and some overestimation was observed for the smaller studied reservoir (Bravura). In addition to the differences in reservoir size, the higher wind speeds observed at the Bravura site, as discussed in Section 3.1, may contribute to these discrepancies in evaporation estimates by the MT method. Regarding the average monthly, the differences were $\pm 1$ mm d$^{-1}$ for all reservoirs.

In this study, due to specific pan settlement on the floating platform, as previously referred in to Section 2.2, the measured evaporation at the pan should be identical to real evaporation over the inundated area at the site. The factors that determine high pan evaporation rates usually observed on terrestrial frameworks are minimized here as the pan was placed offshore, on the floating platform, in contact with the water body surface. The best estimates of evaporation using the PEN method are obtained for reservoirs where the wind speed is consistently lower. This can be attributed to the reduced aerodynamic term in the Penman equation, which leads to smaller evaporation estimates and reduces the bias compared to the BREB values. Reservoirs such as Pego do Altar and Santa Clara exhibit nearly zero bias in evaporation estimates when using the PEN method.

Monthly average evaporation rates estimated by the PT method and BREB show a good fit, and it can be observed that in eight out of nine reservoirs, there is a consistent underestimation of evaporation throughout the year. This finding is contrary to what is typically reported in the literature [8]. The standard coefficient ($\alpha$) value of 1.26 used in the PT method takes into account the proportion of energy mobilized for evaporation through advection [60,61]. However, in our specific conditions, this coefficient seems to be insufficient. The observed underestimations of evaporation using the PT method indicate the need to increase the standard coefficient ($\alpha$) value by 10%, suggesting that moderate advection occurs at the reservoir sites.

The THOR method, based on the Thornthwaite formula using air temperature measurements only, tended to underestimate evaporation during the dry semester in most reservoirs, except for Maranhão and Pego do Altar, where the fit was good. The underestimation was more pronounced in the Bravura and Santa Clara reservoirs, with average biases of $-1.10$ mm d$^{-1}$ and $-1.04$ mm d$^{-1}$, respectively.

In the PE method, the trend lines closely align with the 1:1 line, indicating a strong positive correlation between pan measured evaporation and BREB estimated evaporation

for eight reservoirs ($R^2$ values greater than 0.95). However, in the Maranhão reservoir, the pan measured evaporation exceeded the estimated evaporation by 24%. When considering the average monthly difference, there is nearly zero annual bias in most reservoirs except for the Bravura and Maranhão reservoirs. In Bravura, the dry semester exhibits the highest negative bias ($-1.38$ mm d$^{-1}$), while in Maranhão, the maximum bias is positive (0.59 mm d$^{-1}$), also occurring in the dry semester.

Figure 11 shows the average and standard deviation of the monthly differences between BREB evaporation values and estimates obtained from the five alternative evaporation methods. All methods yield evaporation estimates identical to BREB values during the wet semester regardless of the reservoir considered. In the dry semester, all methods provide small biases, but the standard deviations vary substantially depending on the reservoir. Larger standard deviations can be observed in the MT evaporation estimates for the Bravura reservoir and in the PEN values for the Maranhão and Pego do Altar reservoirs.

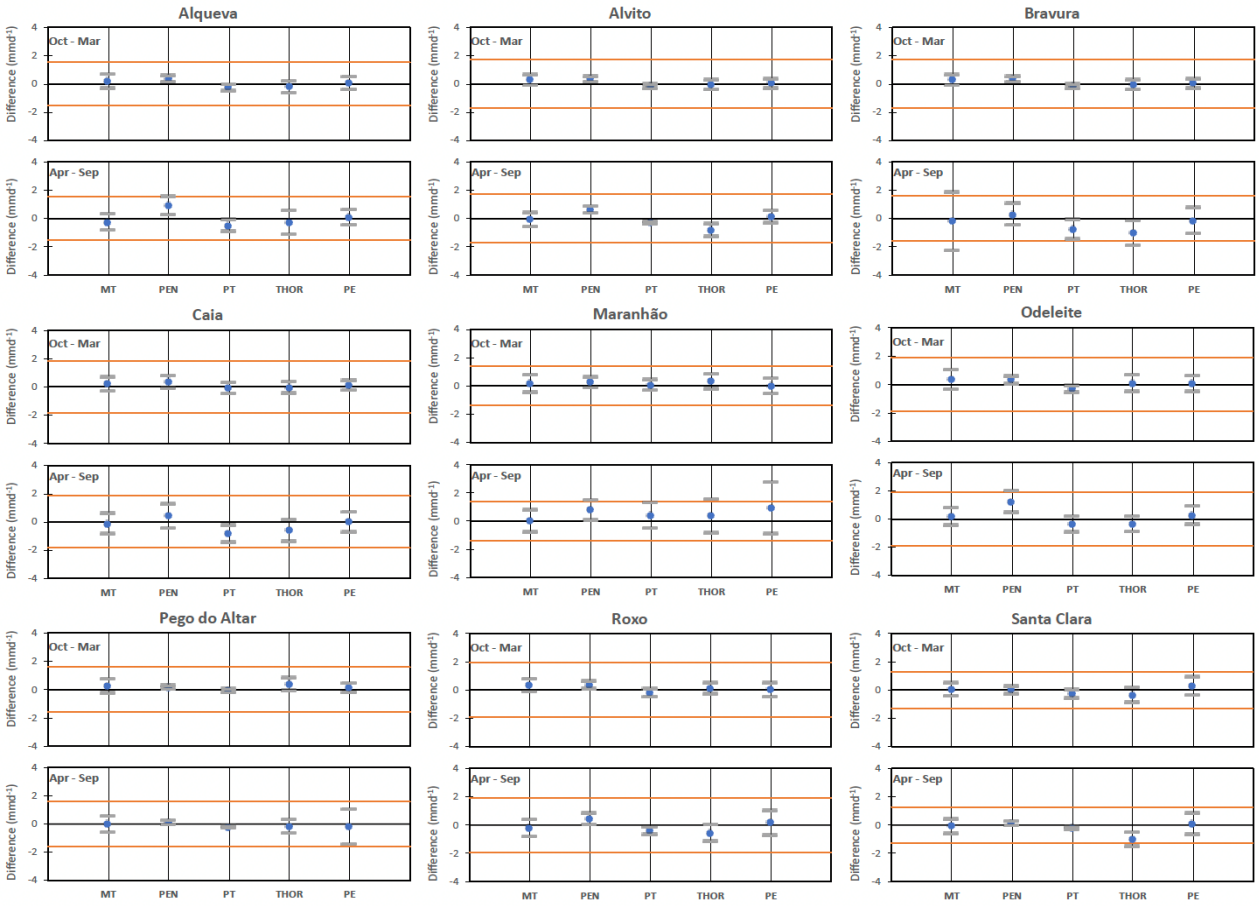


**Figure 11.** Seasonal mean and ±standard deviation of the differences between the monthly estimates of the alternate evaporation methods and the BREB method at all reservoirs. The two orange lines display the standard deviation value associated with the BREB daily estimates.

The evaluation of evaporation methods is presented using the statistical descriptors in Table 3. Table 8 provides the statistics and performance of the methods for all reservoirs. The MT method exhibits the highest Root Mean Square Error (RMSE) value of 1.6 mm d$^{-1}$ in the Bravura reservoir, while the PEN method shows the lowest value of 0.16 mm d$^{-1}$ in the Pego do Altar reservoir. The range of RMSE varies from 0.25 to 0.44 mm d$^{-1}$ for most reservoirs, except for Santa Clara and Bravura, which have values of 0.73 mm d$^{-1}$ and 0.95 mm d$^{-1}$, respectively.

**Table 8.** Statistical descriptors of monthly evaporation (mm $d^{-1}$) and methods performance for the nine reservoirs.

| Reservoir | Method | RMSE | R | IOA | d | Performance |
|---|---|---|---|---|---|---|
| Alqueva | MT | 0.57 | 0.93 | 0.96 | 0.89 | Excellent |
| | PEN | 0.80 | 0.98 | 0.95 | 0.92 | Excellent |
| | PT | 0.57 | 0.97 | 0.96 | 0.94 | Excellent |
| | THOR | 0.73 | 0.90 | 0.94 | 0.84 | Very Good |
| | PE | 0.49 | 0.95 | 0.97 | 0.92 | Excellent |
| Alvito | MT | 0.48 | 0.96 | 0.98 | 0.94 | Excellent |
| | PEN | 0.49 | 0.99 | 0.98 | 0.98 | Excellent |
| | PT | 0.32 | 1.00 | 0.99 | 0.99 | Excellent |
| | THOR | 0.75 | 0.97 | 0.94 | 0.91 | Excellent |
| | PE | 0.39 | 0.98 | 0.99 | 0.96 | Excellent |
| Bravura | MT | 1.60 | 0.74 | 0.82 | 0.61 | Average |
| | PEN | 0.65 | 0.93 | 0.96 | 0.89 | Excellent |
| | PT | 0.92 | 0.92 | 0.90 | 0.83 | Very Good |
| | THOR | 1.16 | 0.87 | 0.83 | 0.72 | Good |
| | PE | 0.78 | 0.87 | 0.93 | 0.81 | Very Good |
| Caia | MT | 0.64 | 0.94 | 0.97 | 0.91 | Excellent |
| | PEN | 0.75 | 0.94 | 0.96 | 0.91 | Excellent |
| | PT | 0.82 | 0.95 | 0.94 | 0.89 | Excellent |
| | THOR | 0.77 | 0.93 | 0.95 | 0.88 | Excellent |
| | PE | 0.56 | 0.95 | 0.98 | 0.93 | Excellent |
| Maranhão | MT | 0.69 | 0.87 | 0.93 | 0.81 | Very Good |
| | PEN | 0.77 | 0.92 | 0.93 | 0.85 | Excellent |
| | PT | 0.72 | 0.88 | 0.94 | 0.83 | Very Good |
| | THOR | 0.61 | 0.88 | 0.93 | 0.82 | Very Good |
| | PE | 0.90 | 0.89 | 0.90 | 0.80 | Very Good |
| Odeleite | MT | 0.64 | 0.94 | 0.97 | 0.91 | Excellent |
| | PEN | 1.01 | 0.98 | 0.94 | 0.92 | Excellent |
| | PT | 0.57 | 0.98 | 0.98 | 0.95 | Excellent |
| | THOR | 0.62 | 0.95 | 0.97 | 0.92 | Excellent |
| | PE | 0.60 | 0.95 | 0.97 | 0.93 | Excellent |
| Pego do Altar | MT | 0.53 | 0.94 | 0.97 | 0.90 | Excellent |
| | PEN | 0.16 | 1.00 | 1.00 | 0.99 | Excellent |
| | PT | 0.24 | 1.00 | 0.99 | 0.99 | Excellent |
| | THOR | 0.51 | 0.95 | 0.97 | 0.92 | Excellent |
| | PE | 0.41 | 0.96 | 0.98 | 0.94 | Excellent |
| Roxo | MT | 0.59 | 0.95 | 0.97 | 0.93 | Excellent |
| | PEN | 0.50 | 0.99 | 0.98 | 0.97 | Excellent |
| | PT | 0.45 | 0.99 | 0.98 | 0.97 | Excellent |
| | THOR | 0.68 | 0.95 | 0.96 | 0.91 | Excellent |
| | PE | 0.70 | 0.94 | 0.97 | 0.91 | Excellent |
| Santa Clara | MT | 0.49 | 0.92 | 0.96 | 0.89 | Excellent |
| | PEN | 0.22 | 0.99 | 0.99 | 0.98 | Excellent |
| | PT | 0.37 | 0.99 | 0.98 | 0.97 | Excellent |
| | THOR | 0.95 | 0.90 | 0.80 | 0.72 | Good |
| | PE | 0.68 | 0.85 | 0.91 | 0.78 | Very Good |

The ranking of methods was determined based on the Index of Performance (*d*) (Table 8) and the Taylor diagram [62] (Figure 12).

The performance of the five methods was classified as *Excellent* for the Alvito, Caia, Odeleite, Pego do Altar and Roxo reservoirs. The PEN and/or PT methods generally performed better, except for the Caia reservoir, where the PE method showed better performance (Table 8). These findings are consistent with the results from the Taylor diagram (Figure 12).

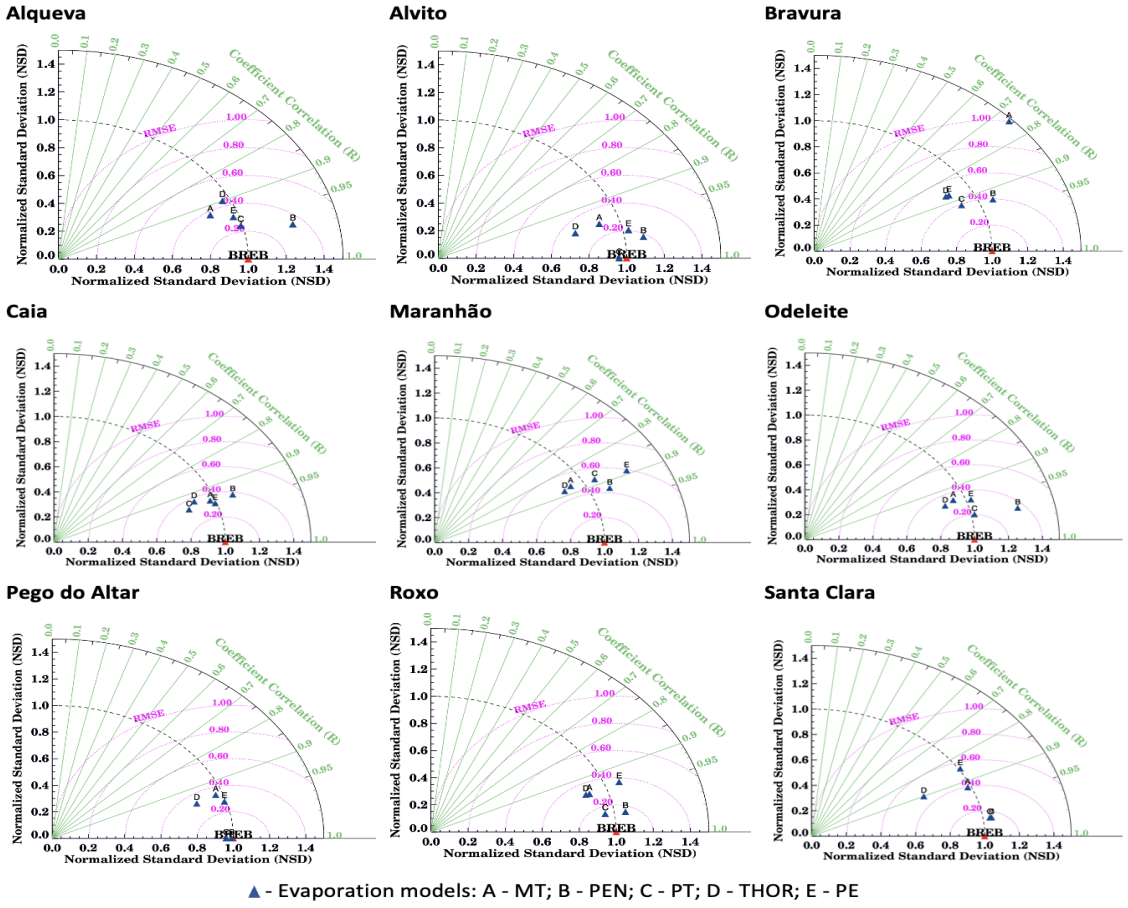


**Figure 12.** Taylor diagram for the nine reservoirs showing the relative *performance* of the five evaporation methods compared to the BREB. The RMSE is indicated by pink arcs, the black arc refers to the NSD, and the green contours indicate the R. The five evaporation methods were assigned by letters.

The Taylor diagram enables stakeholders to identify the better method to apply by considering the study objectives, data availability, and time scale. For instance, in the Alqueva reservoir, the PT, THOR, and PE methods provide an excellent representation of variability, although the PEN method shows a stronger correlation. In Pego do Altar, the PEN and PT methods achieve a correlation coefficient and an NSD equal to one, with an RMSE close to zero, indicating an almost perfect agreement with the observed data.

## 4. Conclusions

This study presents a set of offshore meteorological data—namely, pan evaporation, downward solar radiation, atmospheric pressure, precipitation, air temperature, air relative humidity, wind speed, wind direction, and reservoir water temperature on different levels (1, 5, 10, 15, and 20 m)—obtained in nine meteorological and water temperature floating stations built in nine reservoirs located in southern Portugal. The nine reservoirs are Alqueva, Alvito, Bravura, Caia, Maranhão, Odeleite, Pego do Altar, Roxo, and Santa Clara.

At an annual scale, the simplified four-term energy balance model accurately represented the evaporation process in the reservoirs. There are three exceptions: Bravura, Caia and Maranhão that must be carefully considered.

The monthly analysis of the heat budget revealed significant variations in the latent heat flux ($\lambda E$), which closely aligned with the changes in net radiation ($Q_n$). The peak values of $\lambda E$ generally occurred shortly after the $Q_n$ peak values, indicating a slight time lag. On the other hand, the minimum $\lambda E$ flux was predominantly influenced by the heat storage change ($\Delta Q$) within the reservoir system. Most reservoirs exhibited an annual $\Delta Q$

approaching zero, indicating a null balance between energy gains and losses throughout the years. The sensible heat flux ($H$) showed relatively low values compared to other components of the energy balance. Reservoir evaporation losses demonstrate noticeable seasonal and spatial variations. The results reveal a clear seasonal pattern, with July consistently exhibiting the highest evaporation values, while January experiences the lowest rates. Across all reservoirs, the monthly evaporation varies from 0.8 mm $d^{-1}$ in winter to 4.0 mm $d^{-1}$ in summer with an average of 2.7 mm $d^{-1}$. The northern part of the region consistently exhibits a minimum evaporation throughout the year, while the southwest Algarve region shows maximum values. This spatial pattern remains consistent during both the dry and wet seasons. The annual evaporation values span from 750 to 1230 mm, indicating a significant positive gradient from the northern part of the region toward the southwest Algarve.

Water reservoir managers often do not have access to these data; for that reason a benchmarking analysis of indirect methods [Mass Transfer (MT), Penman (PEN), Priestley and Taylor (PT), Thornthwaite (THOR), and Pan Evaporation (PE)] was carried out. The performance of the methods was evaluated by the $d$ index and the Taylor diagram. Concerning the MT method, an equation for the mass transfer coefficient ($N$) function of the reservoir water surface area ($A_s$) was established for each reservoir, and a general overall equation to Mediterranean climate region was established, too. The reservoir evaporation estimated by the MT method showed a strong correlation with the Bowen Ratio Energy Budget (BREB) method, indicating its accuracy in estimating evaporation rates. However, slight underestimation was observed in the largest reservoir (Alqueva), and there was some overestimation in the smaller reservoir (Bravura), which may be attributed to differences in wind speed and reservoir size. The PEN method overestimated the annual evaporation rates, particularly during the dry season. The best estimates were observed for reservoirs with lower wind speeds, suggesting that the reduced aerodynamic term in the Penman equation contributed to smaller evaporation estimates. The PT method consistently underestimated evaporation rates throughout the year for most reservoirs, being more pronounced in the Bravura and Santa Clara reservoirs. The THOR method showed a tendency to underestimate the evaporation rate during the dry semester for most reservoirs, except for the Maranhão and Pego do Altar reservoirs. The offshore measured PE rates showed a strong positive correlation with the BREB estimated evaporation rates for most reservoirs, demonstrating that it is a good practice to build a offshore pan evaporation.

**Author Contributions:** C.M.R.: Conceptualization, Methodology, Data curation, Writing—review and editing. R.C.G.: Software, Methodology, Writing—review and editing. M.M.: Methodology, Writing—review and editing. All authors have read and agreed to the published version of the manuscript.

**Funding:** This work is funded by National Funds through FCT–Foundation for Science and Technology under the Project UID/05183/2025.

**Data Availability Statement:** The data used in this study are publicly available from the National Water Resources Information System (SNIRH), managed by the Portuguese Environment Agency (APA), at https://snirh.apambiente.pt, last accessed: 21 March 2025.

**Acknowledgments:** The authors acknowledge the R&D unit MED–Mediterranean Institute for Agriculture, Environment and Development (https://doi.org/10.54499/UIDB/05183/2020 (accessed on 17 November 2025); https://doi.org/10.54499/UIDP/05183/2020 (accessed on 17 November 2025)) and the Associate Laboratory CHANGE–Global Change and Sustainability Institute (https://doi.org/10.54499/LA/P/0121/2020 (accessed on 17 November 2025)).

**Conflicts of Interest:** The authors declare no conflicts of interest.

## References


1. Lionello, P. (Ed.) *The Climate of the Mediterranean Region: From the Past to the Future*; Elsevier: Amsterdam, The Netherlands, 2012; ISBN 978-0-12-416042-2.
2. Hoekstra, A.Y.; Mekonnen, M.M.; Chapagain, A.K.; Mathews, R.E.; Richter, B.D. Global monthly water scarcity: Blue water footprints versus blue water availability. *PLoS ONE* **2012**, *7*, e32688. [CrossRef]
3. Alcon, F.; García-Bastida, P.; Soto-García, M.; Martínez-Alvarez, V.; Martin-Gorriz, B.; Baille, A. Explaining the performance of irrigation communities in a water-scarce region. *Irrig. Sci.* **2017**, *35*, 193–203. [CrossRef]
4. Tomas-Burguera, M.; Vicente-Serrano, S.M.; Grimalt, M.; Beguería, S. Accuracy of reference evapotranspiration (ETo) estimates under data scarcity scenarios in the Iberian Peninsula. *Agric. Water Manag.* **2017**, *182*, 103–116. [CrossRef]
5. Rivas-Tabares, D.; Tarquis, A.M.; Willaarts, B.; De Miguel, Á. An accurate evaluation of water availability in sub-arid Mediterranean watersheds through SWAT: Cega-Eresma-Adaja. *Agric. Water Manag.* **2019**, *212*, 211–225. [CrossRef]
6. Mady, B.; Lehmann, P.; Gorelick, S.M.; Or, D. Distribution of small seasonal reservoirs in semi-arid regions and associated evaporative losses. *Environ. Res. Commun.* **2020**, *2*, 061002. [CrossRef]
7. Rodrigues, C.M.M. Cálculo da Evaporação de Albufeiras de Grande Regularização do sul de Portugal. Ph.D. Thesis, Universidade de Evora, Evora, Portugal, 2009. Available online: http://hdl.handle.net/10174/11108 (accessed on 28 April 2023). (In Portuguese)
8. Rosenberry, D.O.; Winter, T.C.; Buso, D.C.; Likens, G.E. Comparison of 15 evaporation methods applied to a small mountain lake in the northeastern USA. *J. Hydrol.* **2007**, *340*, 149–166. [CrossRef]
9. Yao, H. Long-term study of lake evaporation and evaluation of seven estimation methods: Results from Dickie Lake, South-Central Ontario, Canada. *J. Environ. Prot.* **2009**, *1*, 1. [CrossRef]
10. Simon, E.; Mero, F. A simplified procedure for the evaluation of the Lake Kinneret evaporation. *J. Hydrol.* **1985**, *78*, 291–304. [CrossRef]
11. Assouline, S.; Mahrer, Y. Evaporation from Lake Kinneret: 1. Eddy correlation system measurements and energy budget estimates. *Water Resour. Res.* **1993**, *29*, 901–910. [CrossRef]
12. Finch, J.W.; Hall, R.L. *Estimation of Open Water Evaporation: A Review of Methods*; R&D Technical Report W6-043/TR; Environment Agency: Bristol, UK, 2001.
13. Bowen, I.S. The ratio of heat losses by conduction and by evaporation from any water surface. *Phys. Rev.* **1926**, *27*, 779. [CrossRef]
14. Elsawwaf, M.; Willems, P.; Pagano, A.; Berlamont, J. Evaporation estimates from Nasser Lake, Egypt, based on three floating station data and Bowen ratio energy budget. *Theor. Appl. Climatol.* **2010**, *100*, 439–465. [CrossRef]
15. Harbeck, G.E. *A Practical Field Technique for Measuring Reservoir Evaporation Utilizing Mass-Transfer Theory*; U. S. Geological Survey Professional Paper Nº272-E; United States Government Printing Office: Washington, DC, USA, 1962; pp. 101–105.
16. Fritschen, L.J.; Simpson, J.R. Surface energy and radiation balance systems: General description and improvements. *J. Appl. Meteorol. Climatol.* **1989**, *28*, 680–689. [CrossRef]
17. Todd, R.W.; Evett, S.R.; Howell, T.A. The Bowen ratio-energy balance method for estimating latent heat flux of irrigated alfalfa evaluated in a semi-arid, advective environment. *Agric. For. Meteorol.* **2000**, *103*, 335–348. [CrossRef]
18. Harbeck, G.E. *Water-Loss Investigations: Lake Mead Studies*; U. S. Geological Survey Professional Paper Nº298; United States Government Printing Office: Washington, DC, USA, 1958; pp. 29–35.
19. Sturrock, A.; Winter, T.; Rosenberry, D. Energy budget evaporation from Williams Lake: A closed lake in north central Minnesota. *Water Resour. Res.* **1992**, *28*, 1605–1617. [CrossRef]
20. Lenters, J.D.; Kratz, T.K.; Bowser, C.J. Effects of climate variability on lake evaporation: Results from a long-term energy budget study of Sparkling Lake, northern Wisconsin (USA). *J. Hydrol.* **2005**, *308*, 168–195. [CrossRef]
21. Winter, T.C. Uncertainties in estimating the water balance of lakes 1. *J. Am. Water Resour. Assoc.* **1981**, *17*, 82–115. [CrossRef]
22. Penman, H.L. Natural evaporation from open water, bare soil and grass. *Proc. R. Soc. London Ser. A Math. Phys. Sci.* **1948**, *193*, 120–145. [CrossRef]
23. Brutsaert, W. *Evaporation into the Atmosphere: Theory, History, and Applications*; Springer: Berlin/Heidelberg, Germany, 1982; p. 299.
24. Priestley, C.H.B.; Taylor, R. On the assessment of surface heat flux and evaporation using large-scale parameters. *Mon. Weather. Rev.* **1972**, *100*, 81–92. [CrossRef]
25. Stewart, R.B.; Rouse, W.R. A simple method for determining the evaporation from shallow lakes and ponds. *Water Resour. Res.* **1976**, *12*, 623–628. [CrossRef]
26. Thornthwaite, C.W. An approach toward a rational classification of climate. *Geogr. Rev.* **1948**, *38*, 55–94. [CrossRef]
27. Mather, J.R. *The Climatic Water Budget in Environmental Analysis*; Lexington Books: Lexington, KY, USA, 1978; p. 239.
28. Palmer, W.C.; Havens, A.V. A graphical technique for determining evapotranspiration by the Thornthwaite method. *Mon. Weather. Rev.* **1958**, *86*, 123–128. [CrossRef]
29. Hounam, C. *Comparison Between Pan and Lake Evaporation*; Technical Note Nº126; World Meteorological Organization: Geneva, Switzerland, 1973; p. 54.

30. Dalton, J. *Experiments and Observations to Determine Whether the Quantity of Rain and Dew Is Equal to the Quantity of Water Carried Off by the Rivers and Raised by Evaporation: With an Enquiry into the Origin of Springs*; R. & W. Dean: Manchester, UK, 1802.
31. El-Mahdy, M.E.S.; Abbas, M.S.; Sobhy, H.M. Development of mass-transfer evaporation model for Lake Nasser, Egypt. *J. Water Clim. Change* **2021**, *12*, 223–237. [CrossRef]
32. Anderson, E.R. Energy-budget studies. In *Water Loss Investigations—Lake Hefner Studies*; Technical Report, U. S. Geological Survey Professional Paper Nº269; United States Government Printing Office: Washington, DC, USA, 1954; pp. 71–119.
33. Penman, H.L. Vegetation and hydrology. *Soil Sci.* **1963**, *96*, 357. [CrossRef]
34. Linacre, E. *Hydrology. An Introduction*; Cambridge University Press: New York, NY, USA, 2004.
35. Sene, K.; Gash, J.; McNeil, D. Evaporation from a tropical lake: Comparison of theory with direct measurements. *J. Hydrol.* **1991**, *127*, 193–217. [CrossRef]
36. Xu, C.Y.; Singh, V. Evaluation and generalization of radiation-based methods for calculating evaporation. *Hydrol. Processes* **2000**, *14*, 339–349. [CrossRef]
37. Wang, W.; Xiao, W.; Cao, C.; Gao, Z.; Hu, Z.; Liu, S.; Shen, S.; Wang, L.; Xiao, Q.; Xu, J.; et al. Temporal and spatial variations in radiation and energy balance across a large freshwater lake in China. *J. Hydrol.* **2014**, *511*, 811–824. [CrossRef]
38. Linsley, R.K.; Kohler, M.A.; Paulhus, J.L. *Hydrology for Engineers*, 3rd ed.; McGraw-Hill: New York, NY, USA, 1982; p. 512.
39. Abtew, W. Evaporation estimation for Lake Okeechobee in south Florida. *J. Irrig. Drain. Eng.* **2001**, *127*, 140–147. [CrossRef]
40. Tanny, J.; Cohen, S.; Assouline, S.; Lange, F.; Grava, A.; Berger, D.; Teltch, B.; Parlange, M. Evaporation from a small water reservoir: Direct measurements and estimates. *J. Hydrol.* **2008**, *351*, 218–229. [CrossRef]
41. Alazard, M.; Leduc, C.; Travi, Y.; Boulet, G.; Salem, A.B. Estimating evaporation in semi-arid areas facing data scarcity: Example of the El Haouareb dam (Merguellil catchment, Central Tunisia). *J. Hydrol. Reg. Stud.* **2015**, *3*, 265–284. [CrossRef]
42. Rodrigues, C.M.; Moreira, M.; Guimarães, R.C.; Potes, M. Reservoir evaporation in a Mediterranean climate: Comparing direct methods in Alqueva Reservoir, Portugal. *Hydrol. Earth Syst. Sci.* **2020**, *24*, 5973–5984. [CrossRef]
43. Tweed, S.; Leblanc, M.; Cartwright, I. Groundwater–surface water interaction and the impact of a multi-year drought on lakes conditions in South-East Australia. *J. Hydrol.* **2009**, *379*, 41–53. [CrossRef]
44. Dingman, S.L. *Physical Hydrology*, 2nd ed.; Prentice Hall: Hoboken, NJ, USA, 2002.
45. Alvarez, V.M.; González-Real, M.; Baille, A.; Martínez, J.M. A novel approach for estimating the pan coefficient of irrigation water reservoirs: Application to South Eastern Spain. *Agric. Water Manag.* **2007**, *92*, 29–40. [CrossRef]
46. Lowe, L.D.; Webb, J.A.; Nathan, R.J.; Etchells, T.; Malano, H.M. Evaporation from water supply reservoirs: An assessment of uncertainty. *J. Hydrol.* **2009**, *376*, 261–274. [CrossRef]
47. Kohler, M.; Nordenson, T.; Fox, W. *Evaporation from Pans and Lakes*; US Weather Bureau Research Paper 38; US Weather Bureau: Washington, DC, USA, 1955.
48. Shuttleworth, W. *Evaporation: Handbook of Hydrology*; Maidment, D.R., Ed.; McGraw-Hill: New York, NY, USA, 1992.
49. Yihdego, Y.; Webb, J.A. Comparison of evaporation rate on open water bodies: Energy balance estimate versus measured pan. *J. Water Clim. Change* **2018**, *9*, 101–111. [CrossRef]
50. García-López, S.; Salazar-Rojas, M.; Vélez-Nicolás, M.; Isidoro, J.M.; Ruiz-Ortiz, V. Estimation of evaporation in Andalusian reservoirs: Proposal of an index for the assessment and classification of dams. *J. Hydrol. Reg. Stud.* **2025**, *58*, 102224. [CrossRef]
51. Melišová, E.; Vizina, A.; Hanel, M.; Pavlík, P.; Šuhájková, P. Evaluation of evaporation from water reservoirs in local conditions at czech republic. *Hydrology* **2021**, *8*, 153. [CrossRef]
52. McMahon, T.; Peel, M.; Lowe, L.; Srikanthan, R.; McVicar, T. Estimating actual, potential, reference crop and pan evaporation using standard meteorological data: A pragmatic synthesis. *Hydrol. Earth Syst. Sci.* **2013**, *17*, 1331–1363. [CrossRef]
53. McMahon, T.; Finlayson, B.; Peel, M. Historical developments of models for estimating evaporation using standard meteorological data. *Wiley Interdiscip. Rev. Water* **2016**, *3*, 788–818. [CrossRef]
54. Majidi, M.; Alizadeh, A.; Farid, A.; Vazifedoust, M. Estimating evaporation from lakes and reservoirs under limited data condition in a semi-arid region. *Water Resour. Manag.* **2015**, *29*, 3711–3733. [CrossRef]
55. Winter, T.C.; Buso, D.C.; Rosenberry, D.O.; Likens, G.E.; Sturrock, A.J.M.; Mau, D.P. Evaporation determined by the energy-budget method for Mirror Lake, New Hampshire. *Limnol. Oceanogr.* **2003**, *48*, 995–1009. [CrossRef]
56. Camargo, A.d.; Sentelhas, P.C. Avaliação do desempenho de diferentes métodos de estimativa da evapotranspiração potencial no Estado de São Paulo, Brasil. *Rev. Bras. Agrometeorol.* **1997**, *5*, 89–97. (In Portuguese)
57. Bouin, M.N.; Caniaux, G.; Traulle, O.; Legain, D.; Le Moigne, P. Long-term heat exchanges over a Mediterranean lagoon. *J. Geophys. Res. Atmos.* **2012**, *117*, D23104. [CrossRef]
58. Giadrossich, F.; Niedda, M.; Cohen, D.; Pirastru, M. Evaporation in a Mediterranean environment by energy budget and Penman methods, Lake Baratz, Sardinia, Italy. *Hydrol. Earth Syst. Sci.* **2015**, *19*, 2451–2468. [CrossRef]
59. Gianniou, S.K.; Antonopoulos, V.Z. Evaporation and energy budget in Lake Vegoritis, Greece. *J. Hydrol.* **2007**, *345*, 212–223. [CrossRef]

60. Stewart, R.B.; Rouse, W.R. Substantiation of the Priestley and Taylor parameter $\alpha = 1.26$ for potential evaporation in high latitudes. *J. Appl. Meteorol. Climatol.* **1977**, *16*, 649–650. [CrossRef]
61. Finch, J.; Calver, A. *Methods for the Quantification of Evaporation from Lakes: Prepared for the World Meteorological Organization's Commission for Hydrology*; Centre for Ecology and Hydrology: Wallingford, UK, 2008.
62. Taylor, K.E. Summarizing multiple aspects of model performance in a single diagram. *J. Geophys. Res. Atmos.* **2001**, *106*, 7183–7192. [CrossRef]